Dynamical Ventral Tegmental Area Circuit Mechanisms of Alcohol-Dependent Dopamine Release

Matteo di Volo[1,5], Ekaterina O. Morozova[2], Christopher C. Lapish[3], Alexey Kuznetsov[4*], Boris Gutkin[5,6*]

[1]Unité de Neurosciences, Information et Complexité, CNRS, [2]Volen Center for Complex Systems Brandeis University, [3]Addiction Neuroscience Program, Indiana University - Purdue University Indianapolis, [4]Department of Mathematical Sciences, Indiana University - Purdue University Indianapolis, [5] Group for Neural Theory, LNC INSERM U960, DEC Ecole Normale Superieure PSL University, Paris, France [6]Center for Cognition and Decision Making, NRU HSE, Moscow, Russia. *Last two authors contribute equally.

Corresponding author: Boris Gutkin, boris.gutkin@ens.fr

keywords: ventral tegmental area, computational modeling, alcohol, cortical synchrony

---

This is the author's manuscript of the article published in final edited form as:

di Volo, M., Morozova, E. O., Lapish, C. C., Kuznetsov, A., & Gutkin, B. (2019). Dynamical ventral tegmental area circuit mechanisms of alcohol-dependent dopamine release. European Journal of Neuroscience, 0(0). https://doi.org/10.1111/ejn.14147

Abstract

A large body of data has identified numerous molecular targets through which ethanol (EtOH) acts on brain circuits. Yet how these multiple mechanisms interact to result in dysregulated dopamine (DA) release under the influence of alcohol in vivo remains unclear. In this manuscript, we delineate potential circuit-level mechanisms responsible for EtOH-dependent dysregulation of DA release from the ventral tegmental area (VTA) into its projection areas. For this purpose, we constructed a circuit model of the VTA that integrates realistic Glutamatergic (Glu) inputs and reproduces DA release observed experimentally. We modeled the concentration-dependent effects of EtOH on its principal VTA targets. We calibrated the model to reproduce the inverted U-shape dose dependence of DA neuron activity on EtOH concentration. The model suggests a primary role of EtOH-induced boost in the I_h and AMPA currents in the DA firing-rate/bursting increase. This is counteracted by potentiated GABA transmission that decreases DA neuron activity at higher EtOH concentrations. Thus, the model connects well-established in vitro pharmacological EtOH targets with its in vivo influence on neuronal activity. Furthermore, we predict that increases in VTA activity produced by moderate EtOH doses require partial synchrony and relatively low rates of the Glu afferents. We propose that the increased frequency of transient (phasic) DA peaks evoked by EtOH results from synchronous population bursts in VTA DA neurons. Our model predicts that the impact of acute ETOH on dopamine release is critically shaped by the structure of the cortical inputs to the VTA.

Introduction

While ethanol (EtOH) has broad and diffuse actions throughout the brain, its direct effects on dopamine (DA) neurons in the VTA are well-defined (Morikawa & Morrisett, 2010). Increases in VTA DA neuron firing are observed following direct application of EtOH in vitro (Brodie & Appel, 1998) and animals will willingly self-administer EtOH into the posterior pVTA in vivo (Gatto *et al*., 1994; Rodd *et al*., 2004). These observations have led to the hypothesis that the direct effects of EtOH on VTA DA neurons play a key role in the perceived hedonic properties of the drug (Dyr *et al.,* 1993; Gatto *et al*., 1994; Rodd *et al*., 2004) and the initial stages of transition to alcohol use disorder. However, the numerous direct targets of EtOH found in the VTA *in vitro* have not yet been integrated to provide a coherent account of how EtOH alters function of the VTA. Answering this question is critical for understanding how alcohol affects neural circuits that encode reward and motivation and therefore critical to understand the neural underpinnings of addiction.

When measured *in vivo*, ethanol yields concentration-dependent alterations in the firing rate of DA neurons (Gessa et al. 1985 and Mereu *et al*., 1984). EtOH influences DA neuron firing in an inverted-U like manner, where low concentrations increase DA neuron firing and high concentrations decrease firing. Furthermore, acute ethanol administration increases the frequency and amplitude of DA transients in projection areas (Covey *et al*., 2014). These data indicate that, EtOH not only changes the average firing rate of the DA neuron, but also affects burst firing, which is responsible for DA transients. The hypothesis of the current study is that alcohol directly influences the computational properties of the VTA, which leads to dysregulation of DA levels in projection areas.

A significant body of *in vitro* data has identified multiple targets of EtOH in the VTA that affect the intrinsic dynamics of VTA neurons and their inputs. Among intrinsic EtOH targets, its impact on hyperpolarization-activated cyclic nucleotide–gated (HCN) and G protein-coupled inwardly-

rectifying potassium channel (GIRK) currents has been clearly documented (Brodie & Appel, 1998; Kobayashi *et al.*, 1999; Lewohl *et al.*, 1999; Okamoto *et al.*, 2006; McDaid *et al.*, 2008; Aryal *et al.*, 2009; Tateno & Robinson, 2011). As for the synaptic inputs to the VTA, acute EtOH facilitates Glu transmission (Xiao et al. 2009, Ding et al. 2012), increases the AMPA-to-NMDA current ratio (Saal *et al*., 2003) and enhances GABA transmission onto DA neurons (Theile *et al*., 2008; Morikawa & Morrisett, 2010). The model proposed herein is built to directly assess the contributions of these biophysical alterations to tonic and phasic firing of the DA neuron and DA release observed *in vivo*. In particular, we focus on the increase in DA neuron firing rate and bursting observed *in vivo* (Morikawa & Morrisett, 2010) as ethanol-induced bursting is, to our knowledge, not observed in *in vitro* experiments. Our working hypothesis is that DA neuron bursting seen *in vivo* reflects firing rate fluctuations in DA neurons induced by inputs, but not intrinsic bursting seen *in vitro* (Ping and Shepard 1996).

The processes that underlie the computational properties of the VTA are becoming increasingly clear. In particular, the DA neuron is hypothesized to play a critical role in valuing environmental stimuli (Fonzi et al 2017) by performing a subtraction operation that calculates the difference between its excitatory and inhibitory inputs (Eshel et al. 2015). In order to investigate the computational properties of the VTA circuit, we have previously introduced a novel microcircuit model of the VTA (Morozova *et al*., 2016a). This model investigated the factors that control bursting and tonic firing of DA neurons and outlined a mechanism whereby synchronized firing of GABAergic neurons is capable of *increasing* DA neuron bursting (Morozova *et al*., 2016a). The model lead to a prediction of complex computational functions performed by the VTA circuit where the temporal properties of VTA inputs (e.g. synchronization and average level of activity) play a key role in determining how the inputs are mapped to the DA release events. Natural variations of synchrony and activity levels are widely observed during the presentation of environmentally salient stimuli (Buschman et al. 2012, Baker et al. 2001), and our model provided a unique tool to understand how these modulations are processed by VTA microcircuits and

eventually lead to alterations in DA release. In this paper, we investigate how EtOH alters input-driven responses in the VTA neurons. These analyses are critical in order to understand how drugs of abuse alter the reinforcing efficacy of different behavioral events, thus, changing their evaluation and setting the path towards addiction.

In this paper, first we describe the VTA circuit model and analyze how external input proprieties (synchronization and average activity) affect the DA population activity. We then model the modulation produced by principal EtOH targets in the VTA, calibrating our model to reproduce the inverted U-shape dependence of DA neuron average firing rate on the EtOH dose. We show that partial synchrony among Glu inputs to the VTA is essential to reproduce the EtOH dose dependence of DA population firing. Further, the model predicts that the bursts seen in the VTA DA neuron population are due to the synchrony among the Glu inputs, and that EtOH increases this burst firing in a dose-dependent manner. Our simulations show that the mechanism responsible for the elevated DA bursting is the synchronization of the DA neuron population. Furthermore, the increase in DA population bursting produced by EtOH, as predicted by the model, explains EtOH-evoked amplification of DA transients observed in vivo.

Methods

We developed a circuit spiking model of the VTA incorporating a population of DA and a population of GABA neurons (projecting to the DA neurons and interconnected with one another) together with a putative model of inputs to this circuit and its dopamine output. The following subsections describe the structure of the model.

VTA circuit: DA neuron population

In the model we consider heterogeneous population of 100 DA neurons, each one receiving inputs from different subset of GABA neurons and with different leak currents assigned randomly in the interval [0.13:0.23] mS/cm^2. This choice determines DA neurons intrinsic peacemaking activity in

the range of 1-4Hz. The choice of the number of DA and GABA neurons was based on our previous model (Morozova et al. 2017). While this choice has a certain degree of freedom as no clear data, to our knowledge, give such information, the results we describe do not depend qualitatively on this choice.

Each DA neuron is described by a single-compartment biophysically-based model:

$$c_m \frac{dv}{dt} = I_K + I_{Ca} + I_{K,Ca} + I_{sNa} + I_{GIRK} + I_h + I_{leak} + I_{Na} + I_{AMPA} + I_{NMDA} + I_{GABA}$$

Where *v* is the voltage, and the first eight currents represent intrinsic currents: a potassium current I_K, a calcium current I_{Ca}, a calcium-dependent potassium current $I_{K,Ca}$, a subthreshold sodium current I_{sNa}, a G protein-coupled inwardly-rectifying potassium current I_{GIRK}, an H-type hyperpolarization-activated cationic current, a leak current I_{leak} and a sodium current I_{Na}. AMPA and NMDA receptor currents (I_{AMPA} and I_{NMDA}, respectively) model excitatory inputs and GABA receptor current (I_{GABA}) models inhibitory inputs. The intrinsic currents contribute to the excitability and pacemaking mechanisms of DA neuron, while synaptic inputs produce bursts and pauses. Gating of these currents, which follows the standard Hodgkin-Huxley scheme, is described in detail in supplementary material S2 and is based on our previous work (see (Morozova *et al*., 2016a)). Parameters of the currents are given in Table 1.

VTA circuit: GABA neuron population

The circuit contains 50 heterogeneous GABA interneurons, forming a circuit that fires tonically at higher rates around 20Hz (Margolis et al., 2012). The voltage dynamics of each GABA neuron is described by Wang-Buszaki model (see supplementary material S2) with parameters distributed to reflect heterogeneity: Experimental data suggests that the range of firing rates of recorded VTA GABA neurons is very broad with the mean of 19Hz (Steffensen et al., 1998). The differences in frequencies are modeled by changing the leak conductance g_{lg}, according to g_{lg}=0.05+0.05*(*rnd*-

0.5), where g_{lg}=0.05 corresponds to the frequency of 17 Hz. Note that the model can fire at much higher rates in response to excitatory inputs, reflecting the experimental data.

The GABA neurons are interconnected through gap-junctions, in accordance with experimental data (Allison *et al*. 2006) and modeled by the typical electrical coupling function (Kepler et al., 1990). Specifically, each GABA neuron is coupled with all the other neurons in the population with the typical electrical coupling $I_{el}=g_{el}(v_i-v_j)$, where v_i and v_j are the voltages of neurons indexed *i* and *j*.

Intra-circuit coupling: interneuron to DA neuron feed-forward connections

GABA interneurons project to the DA neurons. Inputs from a subpopulation of 10 GABA neurons in the circuit converge on each DA neuron. The GABA gating variable is described by the standard synaptic model (Wang and Buzsaki, 1996) calibrated according to (Richards *et al.,* 1997):

$$\frac{dGABA_i}{dt} = \frac{g_{spike}(v_i)(1 - GABA_i)}{\tau_{gact}} - \frac{(1 - g_{spike}(v_i))GABA_i}{\tau_{gdeact}}$$

$$\text{where} \quad g_{spike} = \frac{1}{1+\exp(-v_i/2)}$$

The overall GABA gating variable for a given DA neuron is an average over M=10 randomly chosen units in the GABA population:

$$GABA(t) = \sum_{i}^{M} GABA_i/M$$

The inhibitory post-synaptic current flowing into the DA neuron is then I_{GABA}= $g_{GABA}GABA(t)(E_{GABA}-v)$, where *v* is the voltage of the DA neuron. The exact number of projecting GABA neurons to DA neurons is not known. As we described in our previous paper (Morozova et al. 2017) and since GABA neurons modulate DA neuron activity through monosynaptic inhibitory connections (Bourdy and Barrot, 2012; van Zessen et al., 2012), one can expect multiple GABA neurons to make connections with a single DA neuron. We made a

judicious choice of GABA to DA convergence and we verified that our results do not depend qualitatively on the specific choice of this number.

Glutamatergic inputs to the circuit

To model the temporal structure of the excitatory synaptic inputs impinging on the VTA microcircuit, we designed a model of spike trains generated by a population of 50 glutamatergic neurons that project to the VTA. These inputs can come from putative cortical pyramidal neurons that project to the VTA and/or glutamatergic neurons from the pontine nuclei. In particular, the inputs could be associated with a newly identified pathway that monosynaptically links fronto-cortical pyramidal neurons to VTA neurons that in turn project to the striatum (Beier et al 2017). The spike trains are characterized by two main parameters: the average level of activity and the synchrony among the spiking units. Each individual unit emits spikes according to a Poisson process with an average firing rate controlled by the parameter ν_{Glu}. To modulate synchrony, we constrain a fraction N_s of units to emit spikes synchronously within a pre-defined time windows of 5 msec. The duration of synchronous and asynchronous intervals is extracted from a Poisson distribution with a mean period T_s=4s. Fig.1A shows example rasterplots of the generated input spike trains with ν_{Glu}=4Hz, N_s=0 (no synchronous units) and 0.14 (units 0 to 7 are synchronous). By changing N_s we can control the fluctuations in the number of spikes in a time bin (e.g. 50ms in Fig. 1A). The generated spike trains are used as input to the VTA through AMPA and NMDA receptors located on both GABA and DA neurons. The dynamics of AMPA and NMDA synapses follow the same dynamical role in both GABA and DA neurons, depending on the receptor type (AMPA or NMDA). Nevertheless, they are different between GABA and DA neurons having different maximal conductances (e.g. $g_{DA,AMPA}$ and $g_{GABA,AMPA}$ for AMPA).

The AMPA synaptic current on a DA neuron is given *by* $I_{AMPA}=g_{AMPA}p_{AMPA}(t)(E_{AMPA}-V(t))$, where g_{AMPA} is the maximal AMPA conductance and $p_{AMPA}(t)$ is the open probability, which depends on the Glu input (see below; we drop the subscript DA here for simplicity). The NMDA conductance has the voltage dependence

$$g_{NMDA}(v) = \frac{\bar{g}_{NMDA}}{1 + 0.1[Mg^{2+}]e^{-m_e v}}$$

where $[Mg^{2+}]$ denotes magnesium concentration, taken to be 1.4 mM (Li *et al*., 1996), and $m_e = 0.062$ as in our previous model (Ha & Kuznetsov, 2013). Similar to the AMPA, the NMDA current is $I_{NMDA}=g_{NMDA}(v)p_{NMDA}(t)(E_{NMDA}-V(t))$.

The open probabilities p_{NMDA} and p_{AMPA} for the synaptic channels are calculated as a product of activation and desensitization gating variables for AMPA, and just equal to the activation variable for NMDA because its desensitization is assumed negligible: $p_{AMPA} = s^{act,AMPA}s^{des,AMPA}$, $p_{NMDA} = s^{act,NMDA}$, where the gating variables obey the equations

$$\frac{ds^{act}}{dt} = \frac{j(1-s^{act})}{\tau_{act}} - \frac{(1-j)s^{act}}{\tau_{deact}},$$

$$\frac{ds^{des}}{dt} = \frac{(1-j)(1-s^{des})}{\tau_{desrel}} - \frac{js^{des}}{\tau_{des}},$$

where, $\tau_{act}, \tau_{deact}, \tau_{desrel}, \tau_{des}$ are timescales of activation, deactivation, desensitization release and desensitization respectively.

The variable *j* follows the time series for the Glu inputs and reflects their nonlinear summation. The nonlinearity reflects the fact that sparse, asynchronous activation of synapses scattered across the dendritic tree will not trigger a somatic spike, whereas, synchronous synaptic activation is required to evoke a spike (Reyes 2001). The dynamics of Glu synaptic concentration is normalized in the model so that each spike in the input increases it by one unit for one msec. The cumulative signal Q(t) is calculated as a sum of these signals from all 50 Glu units and, due to the normalization, equals to the number of spikes the DA neuron receives at time t. We use the sigmoid function $j = 1/\left(1 + e^{-(Q(t)-9)/1.3}\right)$ to model gating of AMPA and NMDA channels. The

constants are calibrated for the channels to open at 4 and higher simultaneous presynaptic spikes. In our previous work (Morozova et al. 2017) the opening was considered as a step function activating at two simultaneous spikes while here we use a continuous activation. This choice allows for summation effects of several spikes instead of a dichotomous role. Nevertheless, both choices (and in particular the amount of spikes for receptor activation) are not driven by clear experimental evidences as, at our knowledge, there are not. In our model, this calibration allows for weak background activation of the AMPA and NMDA gating variables when Glu inputs are asynchronous and firing around $\nu_{Glu} = 4Hz$.

Output from the circuit: DA release

According to Wightman & Zimmerman (1990), the dynamics of the DA concentration in the striatum is described by the following equation:

$$\frac{d[DA]}{dt} = [DA]_{max} \sum_{s} \delta(t - t_s) - \frac{[DA]V_{max}}{K_m + [DA]}$$

The first term describes DA release by DA neurons following spiks at times $\{t_s\}$: the delta function δ $(t\text{-}t_s)$ instantly increases DA concentration by a fraction $[DA]_{max}$ at the time of a spike. The second term models the DA reuptake described by the Michaelis-Menten equation, where V_{max}=0.004 μM /ms is the maximal rate of uptake by the DA transporter in NAcc and K_m=0.2 μM is the affinity of the transporter. In these units, the DA concentration is obtained in μM. The total DA concentration DA_T (see Fig.6) is the linear sum of the dopamine released by each DA neuron $[DA]_i$:

$$DA_T = \sum_i [DA]_i$$

Ethanol effects: EtOH concentration and ETOH effects on model parameters

Ethanol effects are taken into account by modulating the model parameters. It changes the I_h currents maximal conductance, g_h, and the GIRK currents maximal conductance g_{GIRK} (Okamoto *et al*., 2006, McDaid *et al*. 2008). Furthermore, it affects DA neuron AMPA and GABA channel maximal conductances, g_{AMPA} and g_{GABA} (Saal *et al*., 2003; Theile *et al*., 2008; Morikawa & Morrisett, 2010). To implement the simplest smooth dependence of each of these four parameters on EtOH concentration, i.e. the function P([EtOH]) where P stands for g_h, g_{GIRK}, g_{AMPA}, or g_{NMDA}, it is modeled as a sigmoidal function:

$$P(x) = P_0 + \frac{P_M - P_0}{1 + e^{-((x-c_a)/c_s)}}$$

where x indicates the EtOH concentration [EtOH] in g/Kg, P_0 is the parameter value for zero EtOH concentration, P_M the parameter value at saturation (i.e. at high EtOH concentration), c_a indicates the concentration level at which the parameters P becomes affected, and c_s is the slope of the dependence. The values for the parameters of each sigmoid were calibrated by the known range of values for each conductance without EtOH and their changes during EtOH influence from the in vitro experimental literature listed above. They were further adjusted to reproduce the inverted U-shape of the DA neuron firing rate on EtOH dose in vivo (Mereu *et al*., 1984). Specifically, the value of c_s is equal to c_s=0.1 g/Kg for all the parameters P, while c_a= 0.4 g/Kg for all the parameters but GABA conductance for which c_a=0.8 g/Kg. This allows us to separate the excitatory and inhibitory influence of EtOH at growing concentrations. The values of P_0 and P_M are listed in the table of parameters and have been calibrated according to experimental findings (see Result). In particular, we should also note that we calibrated our model to qualitatively reproduce the inverted-U effects of EtOH on DA neuron firing. As such we did not explicitly incorporate differences in the sensitivity to EtOH between the different neuronal populations. However, the EtOH activation function we constructed could be adjusted to reflect differences in sensitivity to EtOH across

neural populations. We expect that, for example, in the case of GABA conductance, the more it is sensitive to ETOH, the more the inhibitory effect of EtOH at high concentration will be pronounced.

DA neuron electrical coupling

Gap junctions between DA neurons have been reported (Grace & Bunney 1993), and we model them as electrical coupling between DA neurons i and j of the form $g_{DA,el}(v_i-v_j)$. For simplicity, we consider all-to-all coupling: any neuron i receives an additional current $I_{DA,el}=g_{DA,el}(v_i-V)$, where V is the average voltage of DA neuron population. The maximal conductance $g_{DA,el}$ is used as a free parameter to study the impact of gap junctions on the DA neuron firing. In Supplementary Fig. S1, we show that the effects of EtOH on the DA neuron firing rate and bursting hold for a wide range of low $g_{DA,el}$ values.

The GIRK current

The GIRK current is a Potassium current whose opening depends on DA concentration, thus creating a functional coupling between DA neurons (Ford et al. 2009). The current is written as $I_{GIRK}=g_{GIRK}S_{D2}(E_K-V)$, where g_{GIRK} is the maximal conductance and V is the neuron voltage. The activation variable S_{D2} incorporates a dependence of the GIRK current conductance on D2 receptor activation and evolves according to the following equation:

$$\frac{dS_{D2}}{dt} = \frac{1 + k_{D2}DA - S_{D2}}{\tau}$$

where τ=500ms, DA is the dopamine level and k_{D2} represents the strength of GIRK modulation by DA concentration. In the Supplementary Fig. S1, we show that the effects of EtOH on the DA neuron firing rate and bursting hold for a wide range of low to intermediate values of k_{D2}. Thus,

in all the simulations reported in Results, we assumed no GIRK modulation by DA (k_{D2}=0 M^{-1}) for simplicity, so that it becomes a potassium leak current.

Burst Analysis

To characterize burst firing of DA neuron we calculate two different measures. The first one is the classical percentage of spikes within a burst (%SWB). This measure is calculated over 5 minutes of simulation time with a minimum 200 spikes in this time interval. Bursts are identified as discrete events consisting of a sequence of spikes with the burst onset defined by two consecutive spikes within an interval less than 80 msec, and the burst termination defined by an interspike interval greater than 160 msec (Grace & Bunney, 1984). The %SWB was calculated as a number of spikes within bursts divided by the total number of spikes. Moreover, we introduced a new measure B_{CV} = CV_{ISI}*SWB, where CV_{ISI} is the coefficient of variation of the Inter-Spike-Interval series of the neuron. The CV_{ISI} measures spike times variability, i.e. CV_{ISI}=0 for a regular tonic firing and CV_{ISI}=1 for a Poisson spike train. The burst measure B_{CV} combines high-frequency firing with high interspike interval variability. In other words, this measure is low if firing is tonic regardless of its rate (as the CV is low) and is high only when spikes are fast and occur in bursts.

Results

1. VTA input-output processing: overview of the circuit model

The computational model constructed herein considers how VTA microcircuit dynamics influence DA neuron firing and how these processes are altered by EtOH. The VTA is modelled as a feed-forward inhibitory network of electrically (gap-junction) coupled inhibitory GABAergic neurons that project to a heterogeneous population of DAergic neurons (Margolis et al. 2012 and Roeper 2013; Steffensen et al. 1998). Experimental observations from Steffensen at al. (1998) suggest that VTA GABA neurons have a heterogeneous firing rate distribution with the mean

around 19Hz. Accordingly, we model GABA neurons to fire with a distribution of different intrinsic frequencies (see Methods) centered around the experimentally observed mean.

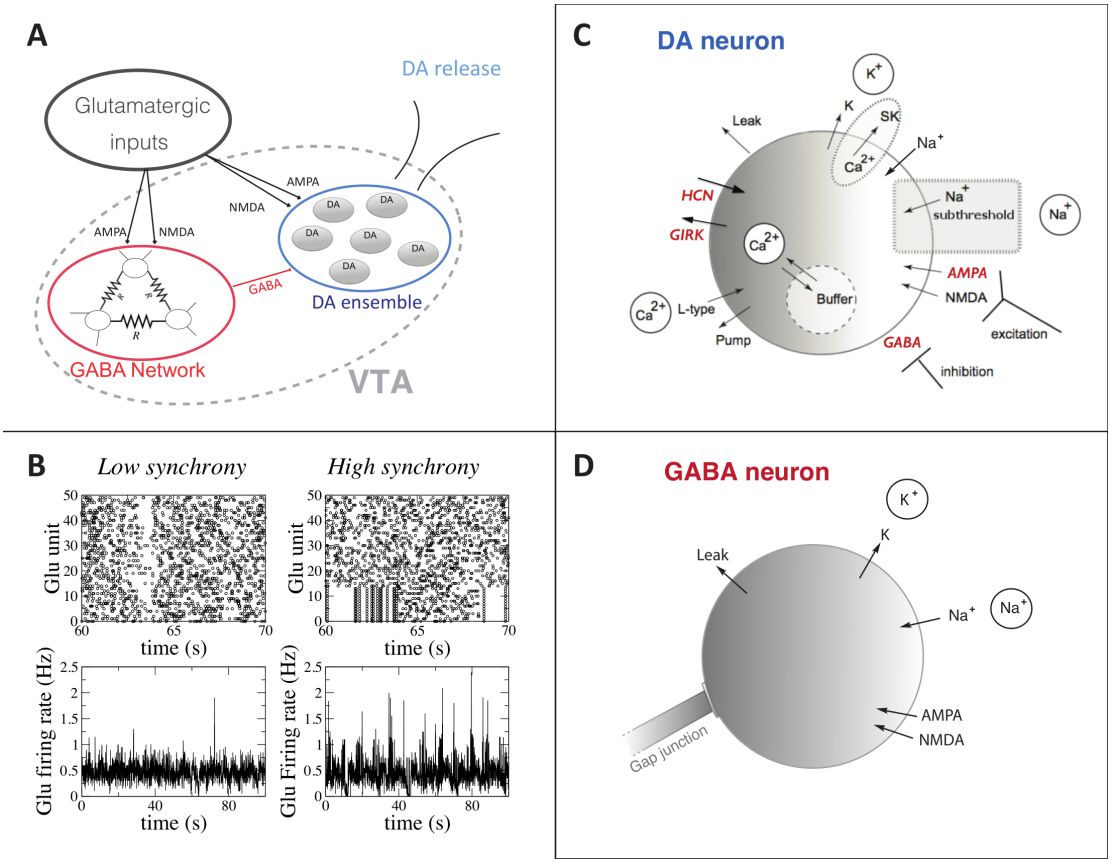

Figure 1: Model description. A) Schematic of the network. Glu inputs project to the VTA, which is composed of a population of electrically connected GABA neurons and a population of DA neurons. B) An example of firing pattern of the Glu units in the asynchronous and weakly synchronous (N_s=16%) cases. The Glu firing rate (bottom) has been calculated through a normalized spike count of the population in a time bin of 10ms. C) Schematic view of an individual DA neuron model. The channels and conductances affected by EtOH are shown in red. D) Schematic view of an individual GABAergic neuron model. ETOH changes the strength of inhibitory projections to the DA neurons. Details of the models are reported in methods section.

Furthermore, the VTA receives excitatory inputs from a number of sources, including from pyramidal neurons of the PFC (Carr & Sesack, 2000) the anterior cortex (Beier et al. 2015); as well as the pedonculopontine tegmentum (Floresco et al. 2003). This excitatory activity furnishes inputs to the VTA through AMPA and NMDA receptors located on both GABA and DA VTA neurons. These inputs project to all GABA and DA neurons but the conductance of DA and GABA neurons receptors is different (see table of parameters). To simulate these Glu inputs, we use a

model that generates 50 Poisson-distributed spike trains with a variable degree of synchronization between them that we define as a free parameter. The choice of Poisson-distributed spike trains is implemented to model the excitatory inputs to the VTA, for example stemming from cortical firing activity (Deghani et al. 2016, Okun et al. 2010).

In order to manipulate the correlations between the Glu neuron spike times we impose a partial synchrony, i.e. we force a fraction $f_s = N_s / N_{Glu}$ of the excitatory inputs to fire within a common 5 ms time window (see method for more details and Fig. 1B as an example). These glutamatergic VTA inputs are thus characterized by two main parameters, the average firing rate (common to all units) ν_{Glu} and their synchronicity N_S. In addition to the Glu inputs, in our model the simulated DA neurons also receive inhibitory inputs from the VTA GABA neurons through $GABA_A$ receptors (see method section, Fig. 1A). The output of the VTA is defined as DA release, which is computed via the model developed by Wightman & Zimmerman (1990; see methods).

Fig.1B shows two examples of the firing pattern of Glu units (asynchronous and partially or weakly synchronous in Fig.1B) with the relative measure of the population firing rate (normalized spike count) showing lower fluctuations in the asynchronous case. In panels C and D we show the model of DA and GABA neurons, described in detail in the method section. Targets of EtOH taken into account in the model are shown in red. Model parameter values are from (Morozova *et al*., 2016a) and listed in table 1, see methods for detailed description.

DA neuron activity depends on Glu input rate and synchronization

To set a baseline for the effects of EtOH, we first analyze processing of Glu input in the VTA circuit model in the absence of EtOH. This will provide a basis to understand the input-output response of the VTA in the presence of EtOH. The two major parameters for the Glu input are its firing rate and the degree of synchrony. We characterize the DA neuron activity response by the firing rate and two measures of variability: the coefficient of variation of the interspike interval (ISI) (CV_{ISI}), and the percent of spikes within bursts (%SWB, Grace and Bunney 1984); see

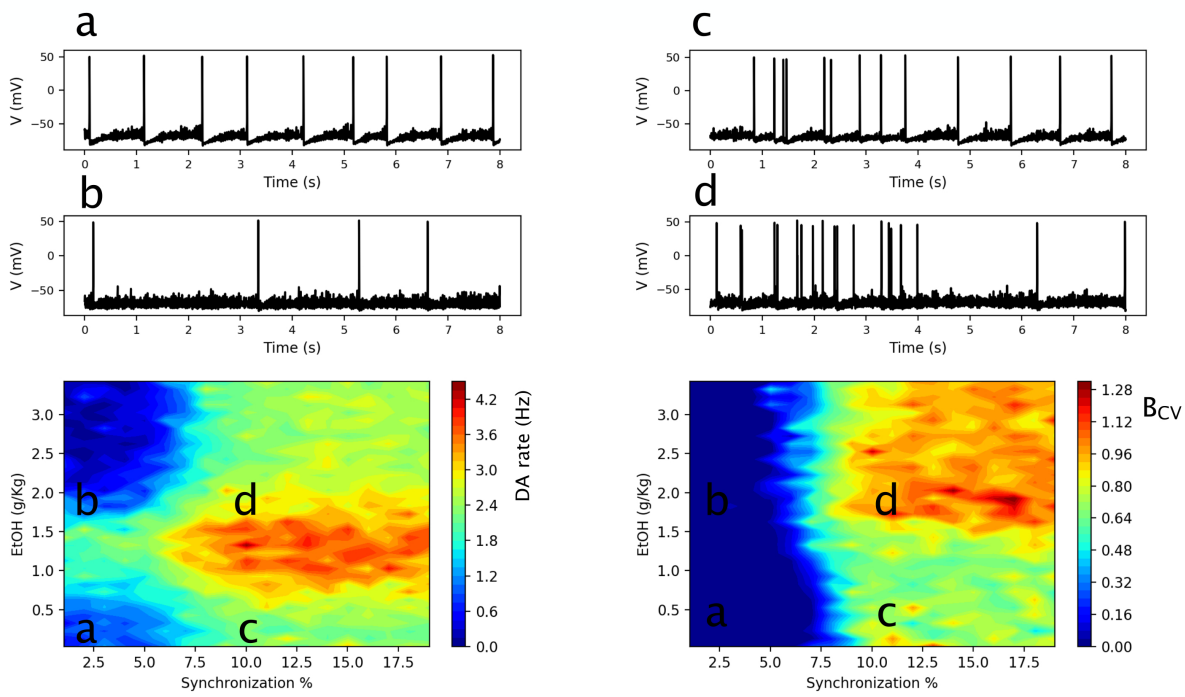

Figure 2: DA neuron activity and Glutamatergic inputs. The heat-maps represent the DA neuron average firing rate (left) and bursting B_{CV} (right) depending on Glu average firing rate and synchronicity. Time traces of DA neuron voltage are shown for the parameter regions as marked (a,b,c,d) in the heatmaps. The activity measures are obtained by averaging simulations over a 200 sec period.

Methods for further details. We also combine these measures and define a burst measure, $B_{CV} = CV_{ISI}*SWB$, which is above zero only for phasic activity at frequencies above 12 Hz. In Fig. 2 we plot the dependence of the firing rate, and the burst measure B_{CV} on the parameters of Glu input synchronization N_s and average rate ν_{Glu}. Shown in Fig. 2 (left panel), the DA neuron average firing rate grows significantly with the growing input rate, yet the growth is only moderate when input synchrony is increased. By contrast, the DA neuron burst measure, B_{CV}, strongly increases when the Glu input becomes more synchronous (Fig. 2, right). In fact, high values of B_{CV} are reached only for a sufficiently strong synchrony (>8%) and a sufficiently low input rate. To illustrate the transitions, we show time traces for the regions of the diagrams marked a, b, c, and d

in Fig. 2. When the input synchrony is low (Fig. 2 a,c) the synaptic input generates an almost tonic current and the DA neuron responds tonically. At the higher input synchrony, the DA neuron firing reflects inhomogeneity in the input (Fig. 1b) as an irregular firing pattern (Fig. 2b). However, at higher average input frequencies the DA neuron is unable to follow the yet greater excitation within the bursts and its firing remains almost tonic. Therefore, the simulations predict that, as Glu afferent activity varies during a behavioral task *in vivo*, the DA neuron activity follows these variations if the input frequency stays below 30Hz.

Calibrating the EtOH dose-dependent effects in the model

We now proceed to determine how EtOH, through its action at the level of the VTA, influences how VTA excitatory inputs are mapped to its outputs (i.e. DA release). For this purpose, we model the most well-validated effects of EtOH on the biophysical properties of VTA neurons:

(1) the DA neuron intrinsic excitability change due to increased HCN (Okamoto et al., 2006) and the GIRK channel conductances (McDaid et al. 2008, see method section).

and

(2) the synaptic effects, i.e. the increase in the GABA conductance as well as in the ratio of AMPA and NMDA synaptic currents in DA neurons (Saal *et al*., 2003; Theile *et al*., 2008; Morikawa & Morrisett, 2010).

DA intrinsic excitability: EtOH affects the intrinsic properties of DA neurons by increasing the maximal conductance of the GIRK and the HCN currents. Fig. 3a shows the effects of changing g_h and g_{GIRK} on the DA neuron firing rate in the model. The increase in g_h has a nonmonotonic effect: an initial increase (0-2 nS/cm^2) increases DA neuron firing rate (up to 150%), whereas at high values of g_h (2-4 nS/cm^2) the firing rate gradually decreases to zero. In vitro EtOH (160 nM)

increases the DA neuron firing rate by approximately 150%; yet when the I_h current is blocked, ethanol produces a decrease in the firing rate (McDaid et al. 2008).

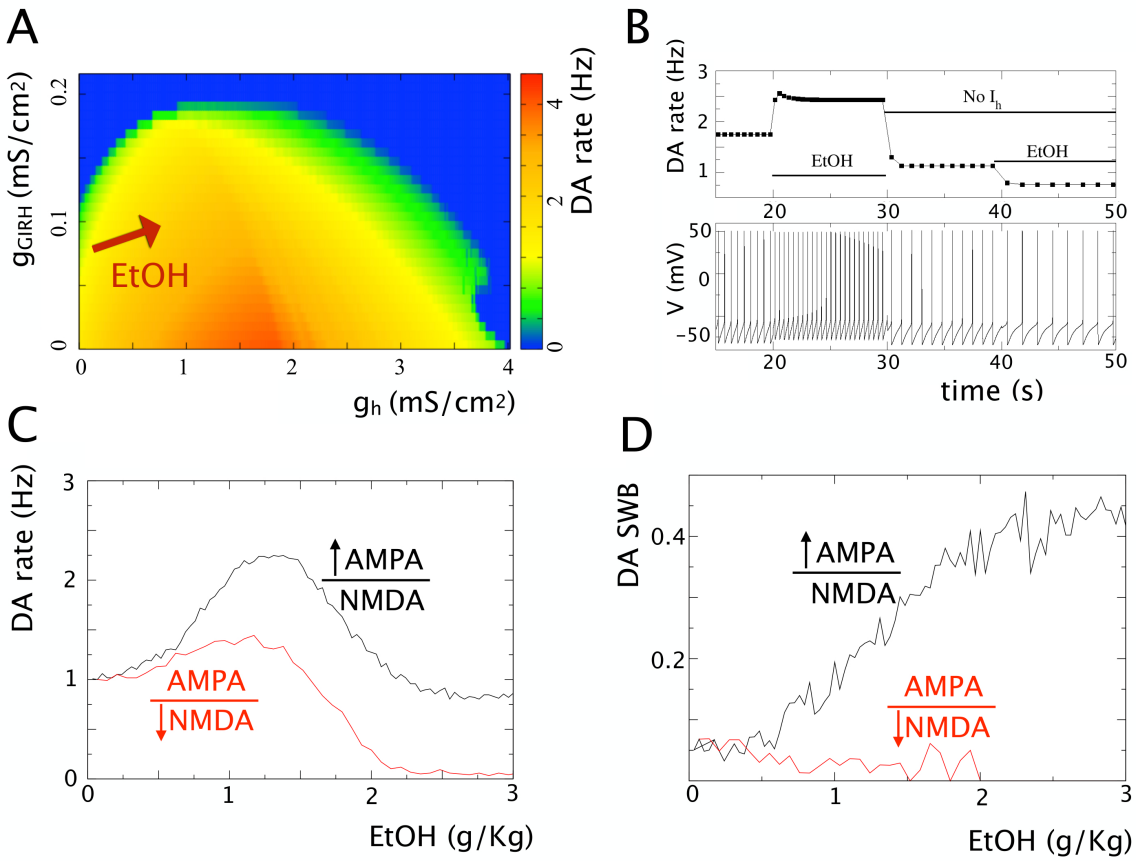

Figure 3. Model calibration for EtOH influence. (A) Combined effect of increasing I_h and GIRK currents on the average firing rate of an isolated DA neuron (no synaptic inputs). The red arrow represents the parameter modulation in EtOH (see Methods for details). (B) Calibration of g_h and g_{GIRK} modulation in the presence of EtOH allows the results by McDaid et al. 2008 to be reproduced: EtOH increases DA firing rate by ~180% and has inhibitory effect when I_h is blocked (C) Dose dependence of DA neuron firing rate on EtOH that reproduces that measured *in vivo* by (Mereu *et al.*, 1984). To match the observed rate growth and the increase in the AMPA/NMDA receptor current ratio measured in vitro (Saal et al. 2003), the AMPA component was amplified (black). The figure also shows that an alternative way to achieve the increase in the AMPA/NMDA ratio by decreasing the NMDAR conductance leads to insufficient increase in the firing rate (red). (D) Dose dependence of DA neuron spike within burst (SWB) on EtOH concentration predicted by the model. Again, black and white curves show the difference in modulating the AMPA vs. modulating the NMDA receptor conductance to manipulate their ratio. Glu input parameters are the same as for the weakly synchronous case in Fig. 1.

We calibrate the modulation of these conductances to reproduce the above results (Fig. 3b). To reproduce the in vitro influence of EtOH (Fig 2b, McDaid et al. 2008), I_h and I_{GRIK} conductanes are modulated as shown by the arrow in Fig. 3a (g_h passes from 0.2mS/cm^2 to 0.8 mS/cm^2 and g_{GIRK} from 0.08 mS/cm^2 to 0.1 mS/cm^2). Through this calibration, we obtain the values for these intrinsic conductances in the DA neuron that correspond to the control conditions and the presence of high EtOH concentration in the slice (equivalent to 160 nM in McDaid et al. 2008). We model the increase of HCN and GIRK conductances with respect to EtOH concentration with a sigmoidal activation function (see methods). This potentiation of the I_h current contributes to the raising phase of the inverted U-shape dependence of the DA neuron firing rate on EtOH dose observed in vivo (Mereau et al. 1984). We have reproduced this dependence (Fig 3c) and normalized the conductance variations by the in vivo dependence, matching the maximum with 1.5 g/Kg EtOH dose (Mereu *et al*., 1984).

Synaptic modulations. To reproduce synaptic EtOH effects, we consider an increase in AMPA/NMDA ratio and an increase in the GABA conductance on DA neurons. The AMPA /NMDA ratio was increased by a factor of 1.5 at an EtOH concentration of 0.02 g/Kg (Saal et al., 2003). As we are considering concentrations up to 2g/Kg we choose an AMPA/NMDA ratio increase up to a factor of four for high EtOH concentrations, that turns out to be enough in order to reproduce the EtOH dose dependence as reported by (Mereu *et al*., 1984). Further, we model the increase in the ratio by the increase in the AMPAR conductance and assume no change in the NMDAR (Ding et al., 2012). To eliminate alternative mechanisms, first, we show in Fig. 3c that decreasing NMDAR conductance does not increase DA neuron firing rate sufficiently. Second, the firing rate increase may also be driven by concurrent increases in the AMPA and NMDA receptor conductances, but their increasing ratio would suggest yet higher increase in the AMPAR conductance, which is more difficult to justify physiologically. Thus the most parsimonious

mechansism for EtOH-mediated increases in firing rate of the DA neuron is increases in AMPA receptor conductance.

Additionally, ethanol enhances GABA transmission onto the VTA DA neurons in vitro primarily via a direct allosteric facilitation of the $GABA_A$ receptors (Theile et al. 2008; see for review Weiner & Valenzuela 2006). We model this influence as an increase in g_{GABA} and calibrate this modulation to reproduce the decreasing phase of the DA neuron firing rate dose dependence on EtOH in (Mereu *et al*., 1984) at concentrations above 2g/Kg. Specifically, we choose the dependence of g_{GABA} on EtOH concentration to activate at higher levels than other EtOH targets (see Methods). Our calibration shows that the above targets are sufficient to reproduce the inverted U-shape dose-dependence of DA neuron activity level on EtOH concentration. We further considered what effect might inter-DA neuron coupling by gap junctions and by D2 autoreceptor activation of the GIRK current have on the DA neuron response to ETOH. Our simulation results (see Fig S1 panels B and C) show that these factors do not alter the results qualitatively. Furthermore, data indicate that DA neuron activity is strongly modulated by NMDA receptors. In the simulations above, we considered AMPA-mediated inputs as the primary vehicle for structuring DA cell activity. To determine if our simulations are compatible with data on NMDA function, we simulated the effects of progressively blocking NMDAR currents in our model. Indeed, DA neuron bursting is prevented by the simulated NMDAR block (see FigS1 A). However, partial decreases in the NMDAR conductance give responses that are decreased in strength (rate and bursting), but follow the general trend of our results above. Other targets may be added to the model later as it is used to answer other questions arising from experiments (Morikawa & Morrisett, 2010).

2. EtOH changes DA activity response to external inputs

To characterize the interaction between Glu excitation and the influence of EtOH on DA neuron activity, we analyze its average firing rate and bursting for different parameters of the Glu signal and EtOH concentrations.

EtOH boosts response to synchronous Glu inputs

First we fix the average rate of Glu excitation (e.g. 4Hz in Fig. 4) to match the background activity levels in the cortex (Deghani et al. 2016; Linsenbardt & Lapish 2015), and vary the synchronization level of the input. The heat-map in Fig. 4 left shows that, while increasing the Glu input synchrony always increases the average DA neuron firing rate (horizontal slice), the inverted U-shape EtOH dose dependence persists for all synchronization levels tested (vertical slice). This dependence can be explained by the amplified endogenous DA cell excitability and Glu synaptic transmission at low EtOH concentrations, and the potentiated GABA transmission at high EtOH concentrations. In more detail, at sufficiently low EtOH concentrations (0-2 g/Kg), the increase in the AMPA and HCN channel conductances by EtOH produces an increase in DA neuron average firing rate. At these concentrations, the GABA receptor conductance is not strongly affected by EtOH. On the contrary, at high EtOH concentrations (2-3g/Kg), the GABAR conductance on the DA neuron becomes sufficiently high to decrease the DA neuron firing rate and eventually (e.g. 3g/Kg) drives it below the values observed at baseline (no EtOH). Thus, the model predicts that the local influence of the EtOH in the VTA on DA neuron excitability and synaptic currents on the DA neurons is sufficient to account for the inverted U-shaped dose dependence observed in-vivo (Mereu *et al*., 1984). We note that this effect is independent of the synchronization level in the Glu inputs.

The heat-map in Fig. 4 right characterizes the DA neuron bursting, B_{CV}, depending on the synchrony of the Glu input and the EtOH concentration. Experiments have shown that EtOH increases bursting in DA neurons (Foddai et al. 2004). Interestingly, our simulations predict that this increase is highly dependent on the synchrony in the Glu drive. At the synchrony levels below 7%, the burst measure stays very low (smaller than 0.05) for any EtOH concentration. Therefore, under the influence of an asynchronous Glu drive, EtOH modulates only the firing rate of the nearly tonic DA neurons (Fig. 4 cases a and b). For higher synchronization levels of Glu inputs (from 7%), the DA neuron firing pattern is characterized by the presence of bursts with a high

intra-burst firing rate (>12 Hz) and periods of tonic activity with low firing frequency (1-6 Hz). EtOH greatly amplifies bursting (Fig. 4, transition c -> d). Interestingly, a hotspot of high bursting activity emerges at high EtOH concentrations (Fig. 4 region d), where the average DA spiking rate is low, and most spikes are thus clustered in bursts.

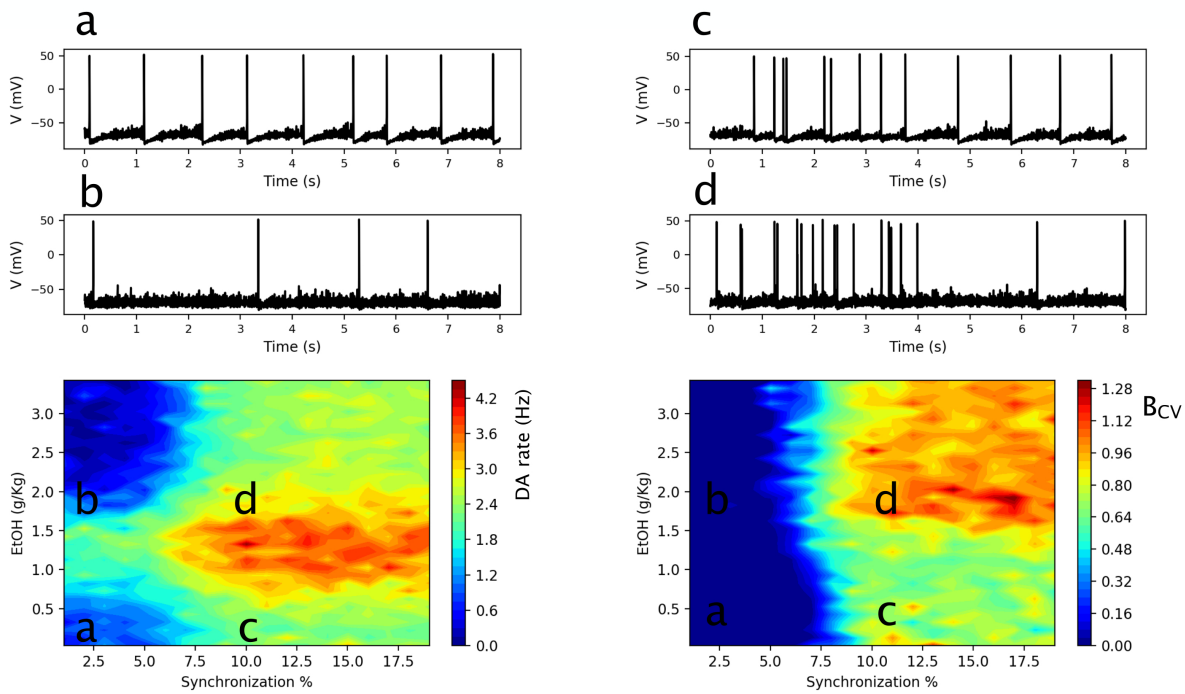

Figure 4: Interaction of EtOH and Glu input synchronization determines DA neuron response. Heat-plots of the DA neuron average firing rates (left) and the burst measure B_{CV} (right) depending on EtOH concentration and synchrony in the Glu input. Time traces of the DA neuron voltage are shown for the parameter regions marked (a,b,c,d) in the heat-plot. The activity measures are averaged over 200 sec simulation.

The mechanism for the EtOH-induced increase in DA neuron bursting can be understood as follows: Our simulations reveal that bursts are produced by episodes of synchronous Glu inputs. The inputs are mediated by NMDA and AMPA receptor activation, yet only AMPAR conductance is affected by EtOH in the model. Thus, EtOH-induced amplification of bursting in DA neurons is mediated by the synchronous AMPA EPSPs. At high EtOH concentrations (e.g. 3g/Kg), an

increase in the GABAR conductance on DA neurons starts to dominate (firing rate decreases, Fig 4 d). Nevertheless, such an increase selectively inhibits tonic DA neuron activity rather than spikes grouped in bursts (also observed experimentally Lobb et al. 2010). In our simulations, this is true for the bursts induced by synchronous AMPAR barrages, for the inhibition of which much higher GABAR conductance values are necessary. As a result, the DA neuron bursts are maintained also at high EtOH concentration, when GABAR conductance is increased, while tonic periods of firing are inhibited. This further boosts the fraction of spikes within bursts at EtOH concentrations that decrease the overall average firing rate. Thus, our model predicts distinct effects of EtOH on tonic and phasic DA neuron firing under partially synchronous Glu inputs.

EtOH inhibits DA activity response to high-frequency Glu inputs

Next, we fix the input synchronization level at 14% (this number permits to obtain EtOH-evoked increase in bursting in DA neurons) and vary the average input rate to model how the influence of EtOH in DA neuron responses depends on this rate. The average firing rate of the DA neuron shown in the heat-map of Fig. 5 left retains the inverted U-shape for a range of low Glu input rates (<20Hz). At higher input rates, it is replaced by a monotonic decrease in the firing rate of the DA neuron (Fig. 5, transition c to d). The mechanism for this change lies in the difference between the influence of pulsatile vs. tonic AMPA receptor current. In vitro studies show that tonic AMPAR activation does not increase the firing frequency of DA neurons (see e.g. (Deister *et al*., 2009)). Our model takes this limitation into account (Ha & Kuznetsov, 2013), but, as shown here, can respond at higher frequency if AMPAR activation is pulsatile. However, at higher input frequencies, the tonic component of AMPA activation increases (data not shown) and impedes repolarizations of the membrane, thus, blocking high-frequency responses. Therefore, the model predicts that EtOH may only inhibit DA neuron firing during time intervals when it is driven by high-frequency Glu inputs (>20Hz).

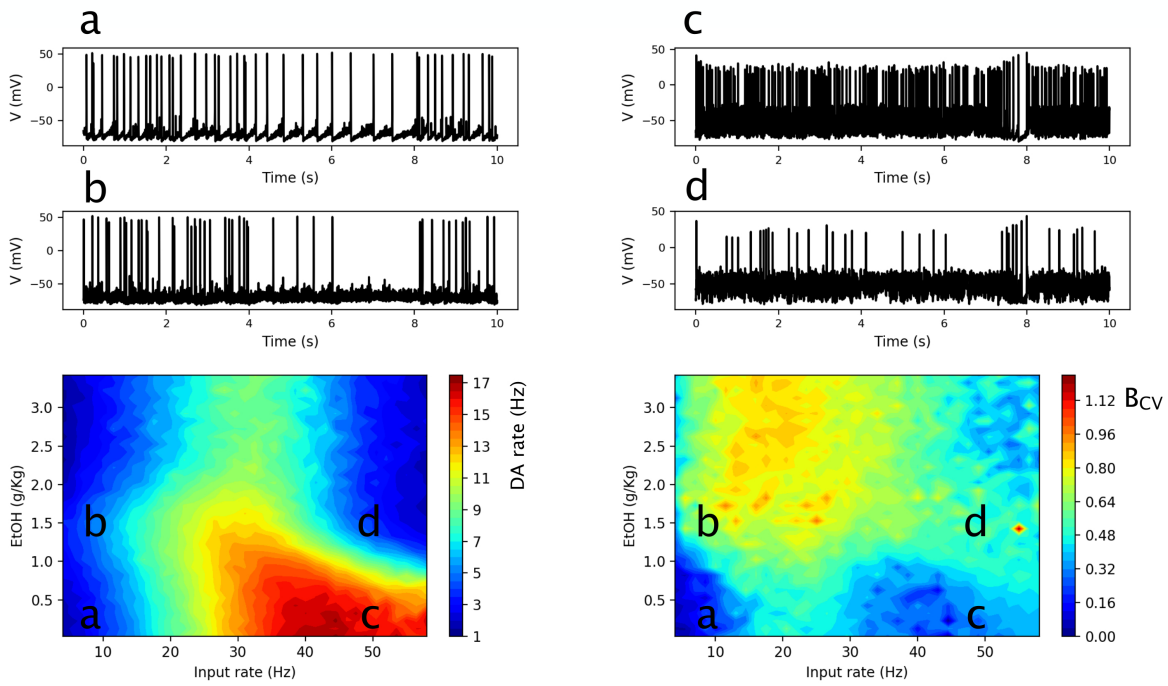

Figure 5: **Interaction of EtOH and Glu input average rate determines DA neuron response.** Heat-plots of the DA neuron average firing rate (left) and the burst measure B_{CV} (right) depending on EtOH concentration and the Glu input rate. Time traces of the DA neuron voltage are shown for the parameter regions marked (a,b,c,d) in the heatplot. The activity measures are averaged over 200 sec simulation.

Bursting of the DA neuron is also low at high-frequency Glu inputs for all EtOH concentrations (heat-map in Fig. 5 right). This result follows directly from those in Fig 2: the DA neuron could not follow the yet greater excitation during the input bursts due to its limited excitability. Some increase in bursting is still achieved at EtOH concentrations around 1.5g/Kg (Fig. 5 transition c to d), and this is mostly due to inhibition of the tonic spiking. This gives a greater contrast between the bursts and the inter-burst tonic firing as described above. At the lower Glu input rates, EtOH causes a much greater increase in the burst measure. The greatest B_{CV} is reached at input frequencies around 10-20 Hz and at EtOH concentrations above 1g/Kg.

3. EtOH amplifies high-concentration DA transients through DA neuron synchronization

The above simulation and analysis establish how acute EtOH together with glutamatergic inputs leads to complex response patterns from single DA neurons. However, the VTA is composed of a heterogeneous population of DA neurons (Lammel et al. 2008, Blythe et al. 2009, Roeper 2013), whose firing activity, collectively, regulates DA release. Multiple currents are differentially expressed in DA neurons which result in heterogeneous excitability properties among the neurons. For simplicity, we modelled such heterogeneity in a population of DA neurons by setting the leak conductances in each DA neuron to a value selected from a uniform distribution in [0.13:0.23] mS/cm^2 range, in order to have a heterogeneous excitability (e.g. firing rate ranges from 0.5 to 3Hz for partially synchronous Glu inputs at 4Hz and no EtOH)). Overall dopamine release was model as a sum of all the dopamine transients produced by individual neurons. We use our simulations to examine our working hypothesis that the significant transient increases observed in the target DA concentrations are due to simultaneous firing of multiple DAergic neurons. Hence we hypothesize that synchronization of the VTA DA neurons is key to DA dynamics. Available data (Lin et al. (2003)) suggests that there are no direct connections among the VTA DA neurons capable of synchronizing them. Hence, it is a common external drive that could act as a synchronizing mechanism. If this drive is tonic, (i.e. the input signal shows little variability due to a low level of synchronization) DA neurons with heterogeneous proprieties will not synchronize their spike times. On the contrary, a transient peak in excitatory input would cause most DA neurons to fire together, thus generating a synchronous population burst.

In order to test this hypothesis, we simulated a heterogeneous population of 100 DA neurons all receiving common partially synchronized glutamatergic inputs (N_s=14%, see Fig.1). The average DA concentration exhibited an inverted U-shape dose dependence on EtOH with a maximum at

an intermediate EtOH concentration around 1.5 g/Kg (see Fig. 6A). The mechanisms behind the inverted U-shape is the same discussed above for the average firing rate of a single DA neuron (see Fig.3), i.e. an increase in each DA neuron firing activity due to HCN and AMPA channel conductance increase at relatively low EtOH concentrations (0-1.5 g/Kg) followed by an activity decrease due to GABA potentiation at higher EtOH concentration (1.5-3 g/Kg).

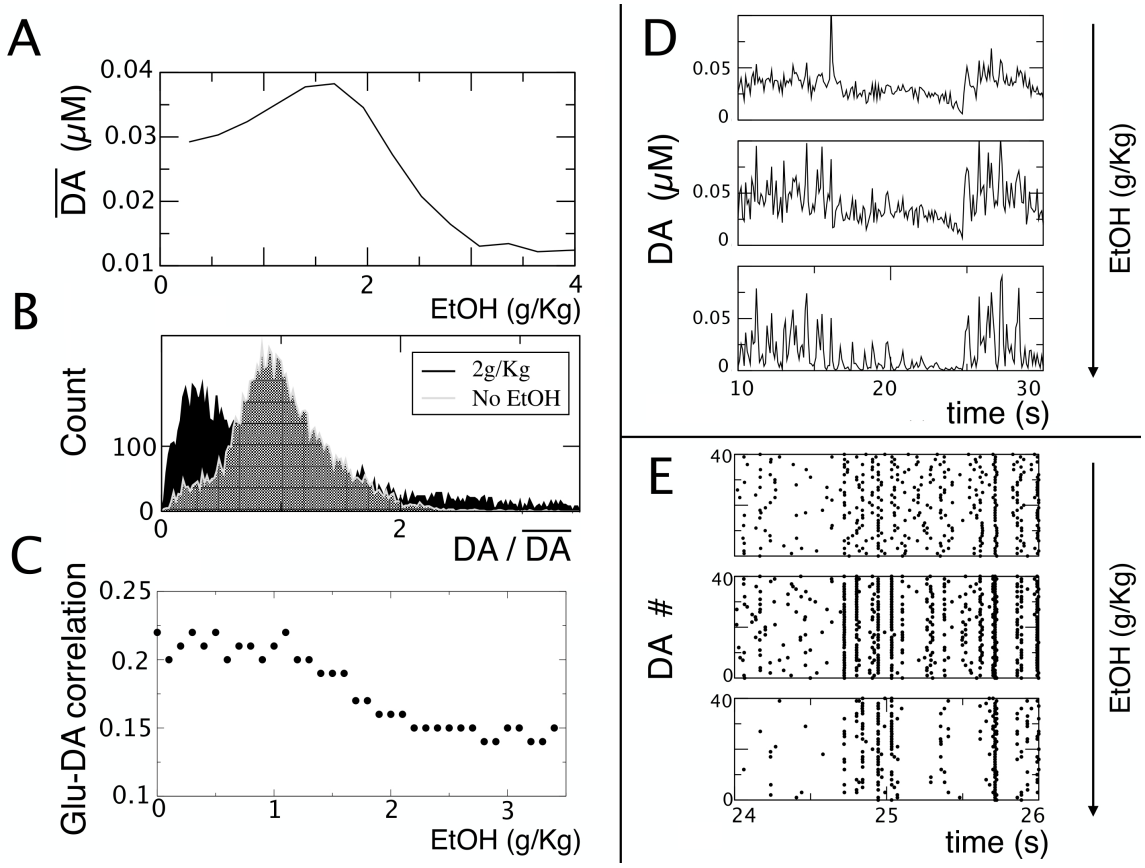

Figure 6. EtOH enhances transient DA peaks by eliciting population bursts of DA neurons.

(A) Average DA concentration ($\overline{DA}$) released by the population of 100 DA neurons at various EtOH concentration. Averaging is over one minute and over all DA neurons in the model. (B) Histogram of the normalized DA concentration DA/ $\overline{DA}$ for two EtOH concentration as reported in the legend. The histogram is calculated by sampling DA concentration time trace with a bin of 100ms (C) The dependence of the Pearson coefficient between Glu input spike count (as in Fig.1B) and DA concentration time trace on EtOH dose. (D) Time trace of DA concentration at the corresponding EtOH doses (0, 2 and 3 g/Kg. (E) Raster plot of a subpopulation of DA neurons at the same EtOH doses. Glutamatergic inputs are partly synchronous (N_s=14%) and ν_{Glu} =14 Hz.

A critically important aspect of DA release, apart from its average level, are transient DA peaks that signal behaviorally-relevant events (Schultz 2002). DA transients are amplified by the majority of addictive drugs (Covey *et al*., 2014). In order to investigate the DA transients, we computed the distribution of DA concentration values over time. In particular, we sampled DA concentration in 180 ms bins and calculated the distribution of the DA levels over an extended period (5 minutes, Fig. 6B). Fig. 6 shows the DA concentration distributions at zero (control) and at an intermediate (2g/Kg) EtOH dose. The distributions are normalized by the mean so that the graph emphasizes the changes in the width. In control conditions, the DA concentrations are Gaussian distributed. At the intermediate ETOH concentration, the distribution has a large tail in the range of high concentrations, meaning that there is a significant number of large-amplitude DA transients. Accordingly, the DA time series (Fig. 6D) shows a clear increase in the temporal variability of DA levels at the intermediate EtOH concentrations. Thus EtOH increases the frequency of large deviations from the basal DA level in the simulations. We observe that in control condition (zero EtOH dose) DA stays at an almost constant level with relatively few peaks. At intermediate EtOH dose, the basal DA level is increased and transient DA peaks are much more frequent (Fig. 6C middle panel). It is crucial to note that for high EtOH concentrations, the basal level of DA is reduced, but the peaks are maintained, yielding a lower DA average level combined with high fluctuations.

To elucidate the mechanism driving these phasic DA events, a raster for the DA neuron population is shown in Fig. 6E. We observed that DA peaks are driven by closely timed spikes in DA neuron population, which can be perceived as population bursts. These events are seldom at low EtOH dose, and therefore DA concentration shows little deviation from the baseline. At higher EtOH dose (1-2g/Kg), the increase in the AMPA conductance permits the AMPA EPSCs to evoke closely-timed spikes in DA neurons, increasing the number of transients (Fig. 6D middle panels, 2g/Kg). The baseline DA level is also increased at this EtOH dose. Together with the stronger

excitatory input, the changes in DA neuron's intrinsic excitability caused by EtOH through I_h potentiation are responsible for this as they increase firing activity throughout the simulation.

At high EtOH doses (EtOH>1.5 g/Kg), the increase in the GABA input inhibits the background asynchronous activity of the DA population. This, in turn, reduces the basal DA levels. Nevertheless, the population bursts of DA neurons are little affected by EtOH-induced inhibition (Fig. 6E bottom). This persistence of population burst and DA transients increasing EtOH doses is consistent with persistence of high burst measures described in previous section (see Fig. 3). Accordingly, at high EtOH doses DA concentrations are characterized by a lower baseline level but still a greater frequency of transient DA peaks. Finally, panel C of Fig. 6 shows the Pearson coefficient between the DA release time trace and the Glu input spike count, measuring their correlation. We observe a decrease in the correlation between Glu input and DA release at high EtOH doses. This is a prediction of the model that could be tested experimentally.

Discussion

Understanding the major factors that control DA signalling and how they are altered by addictive drugs is essential to understand the causes of addiction. A long-standing hypothesis is that ethanol, as well as other drugs of abuse, change the reinforcing value of events and cues by affecting DA signalling (e.g. (Covey *et al*., 2014)). A large body of work has highlighted the multiple and complex ways in which alcohol can influence dopamine circuits and the brain regions they innervate. In this work, we analysed the collective impact of EtOH-related single cell and circuit mechanisms on how the ventral tegmental area processes its input and generates its dopamine output.

While the effects of alcohol on the brain are broad and influence most, if not all, neural circuits, the effects on VTA circuits are direct, robust, and among the most well-validated. Therefore, prior to modelling the broad effects of alcohol on the entire brain it is necessary to first understand how it influences the neural circuits, such as the VTA, where its effects have been

assessed in depth. The goal of the current work was to specifically identify the underlying mechanisms whereby EtOH influences activity of DA neurons in the mesolimbic system. This information provides a more refined understanding of how alcohol alters the integration of afferent signals by the VTA. This is a necessary first step, prior to determining the effects of ethanol on brain-wide activity.

We constructed a computational model of the VTA to determine the critical parameters that control computation in this brain region and how they are influenced by alcohol. This work builds on our previous studies that show how the intrinsic properties of the VTA circuitry, especially synchrony among GABA neurons, play a central role in shaping DA neuron firing and, therefore, DA release throughout the brain (Morozova *et al*., 2016a). Our current work examines *synchrony* in excitatory drive to the VTA and the role it plays in determining DA neuron activity in acute EtOH. Without EtOH, Glu receptor activation in vitro mimics an asynchronous Glu input and excites DA neurons if it affects them directly and inhibits them if it also affects the neighbouring GABA neurons (Paladini and Roeper 2014). Our model reproduces this (Morozova *et al*., 2016a) and shows that Glu input synchrony reverses this inhibition. We observed that Glu synchrony interacts with the direct effects of alcohol on the intrinsic properties of neurons in VTA circuits to blunt background (i.e. tonic) DA release whereas it enhanced evoked (i.e. phasic) release events. Collectively these data indicate that alcohol alters the computational properties of the VTA, which may be critical for the progression toward alcohol abuse. EtOH modulation of the currents and firing patters reproduced in our model suggests a significant role of the AMPA receptors on DA neurons in the amplification of burst firing and DA transients in vivo. A classical view is that NMDA receptors are responsible for burst firing in DA neurons (as in the seminal work by Grace and Bunney 1984; Chergui et al 1993; Overton and Clark 1992). Our model brings together the in vitro data on increasing AMPA/NMDA ratio in EtOH (Saal et al 2003) and in vivo data on increasing DA neuron firing rate and bursting (Meure et al. 1984, Foddai et al. 2004). The model suggests that AMPA contributes to bursting if the excitatory afferents are at least partially synchronous.

Synchrony levels in areas sending Glu projections to the VTA, such as PFC and PPN, are strongly dependent on the behavioral state of the animal (Bushman et al. 2012, Baker et al. 2001). Furthermore, in our simulations, if the NMDAR current is blocked, DA neuron bursting is almost completely abolished (see Supplementary material). Thus, the contribution of AMPA receptors to DA neuron bursting in vivo may have been overlooked. This suggests that in vivo AMPA contribution to bursting mechanism is mediated by dynamical AMPA-NMDA current interaction. In vitro, it has been shown that pulsatile electrical stimulation can trigger firing at intra-burst frequencies in DA neurons that is dependent on AMPA receptor activation (Blythe et al. 2007). Interestingly, a recent paper shows AMPA-evoked bursting in SNc DA neurons in vivo (Galtieri at al. 2017). In vivo, Beier et al (2015) recently showed that stimulation of the frontal cortex leads to dopaminergic responses and is rewarding. Our modelling predicts that the contribution of AMPA receptors to DA neuron firing and, thus, DA transients depends on the behavioral conditions, which modulate synchrony in Glu inputs to the VTA.

In this work, we considered how the structure of the glutamatergic inputs changes the way the DA outflow is modulated by EtOH, or in other words, how ETOH changes DA response to glutamatergic inputs with different structure. Strictly speaking our model is agnostic to the origin of the glutamatergic inputs, as long as they have the requisite average levels and variance. Indeed, these could originate in the cortex and/or a number of subcortical structures furnishing excitatory input to the VTA. One notable example of such is the glutamatergic inputs from the PPN, whose activity tracks salient environmental events and rewards (e.g. Okada et al 2009, Hong and Hikosaka 2014; Keiflin and Janak 2015). Activation of these glutamatergic fibers has been shown to lead to DA neuron activation and DA outflow into the striatum (Pan and Hyland 2005; Blythe 2007). A potential cortical source of excitation to the DA neurons projecting to the NAcc, is the recently identified pathway from the prefrontal cortex (Beier et al 2015). This newly identified pathway has been found to be reinforcing. Hence both of these are perfect candidates for the glutamatergic control over DAergic EtOH reinforcement signalling. In addition, the prefrontal

cortex also sends mono-synaptic projections to the VTA, to both the DA and the GABA neurons, with anatomical studies pointing to a reciprocal DA connection back to the PFC. While unlikely to signal EtOH reinforcement directly, DA modulation in the PFC has been shown to play an important role in controlling neural excitability and neural plasticity (e.g. Gonzales-Burgos et al 2004; see Seamans and Yang 2004 for review) and is likely to play an important function in the formation of representations for EtOH-associated stimuli and goals (Schact et al., 2013; Plassman et al., 2010).

We observed that the frequency of Glu inputs is mainly responsible for the average firing rate of DA neurons and, thus, basal DA levels. Synchrony of Glu inputs predominantly affects bursting and, thus, DA transients. However, our simulations showed that the rich repertoire of VTA DA release dynamics cannot be predicted directly from the Glu input, but rather the VTA local circuit processes these inputs in a complex and nonlinear manner. For example, at VTA DA neuron firing rates below 2Hz, a sharp increase in their bursting can be observed when Glu input synchrony increases by only 2% (8 to 10%) (Fig. 2). This sharp transition suggests that, in this synchrony regime, the DA neurons embedded in the VTA local circuit act as coincidence detectors rather than linear integrators. However, this nonlinearity in bursting is diminished as the firing rate of the Glu input increases, thus indicating that the DA neurons may behave more like linear integrators in this regime. These results highlight the complexity that underlie how Glu inputs are processed by the VTA and underscore the need for approaches that can parse the influence-specific inputs, including GABAergic and modulatory inputs, on computation in the VTA.

The goal of the current study was to tease apart the multiple mechanisms by which acute EtOH altered VTA dynamics. Thus, we further examined the effect of acute EtOH on the computational properties of the VTA. In our model, EtOH targeted the intrinsic properties of DA neurons, notably the I_h current, as well as local circuit parameters, notably, the strength of local GABAergic synapses. In addition, we changed the AMPA/NMDA ratio in the glutamatergic input synapses as compatible with observed data. Our model simulations and analysis lead us to a particularly

striking finding: EtOH amplified the VTA DA neuron population bursting and increased the DA transients only if a certain degree of synchrony was present in the Glu afferents. Another way to interpret our results is that EtOH renders the VTA circuit more sensitive to the synchrony in the Glu afferents, which, in turn, results in more frequent DA transients. Indeed, the burst measure in Fig. 4 shows that, with EtOH, VTA DA neurons start firing in bursts at lower input synchrony, at which the DA neurons remain tonic in the absence of EtOH. The transition occurs at EtOH doses between 1 and 1.5 g/Kg, where EtOH is also most effective in elevating the average firing rate of the DA neurons in our simulations and in the experiments (Mereu *et al*., 1984). Thus we reason that a minimal amount of input synchronization may be necessary to explain the EtOH-evoked increases in the DA cell firing and bursting observed in experiments (Mereu *et al*., 1984; Morikawa & Morrisett, 2010).

It is important to note that in our model the major contribution to DA transients is due to the input-dependent synchronization of the DA neuron population. Input-driven synchronization depends on the temporal structure of the Glu afferents and on the structure of the local GABA-mediated inhibition. We have shown before that synchronous inhibition promotes rapid DA spiking, while asynchronous inhibition inhibits DA firing (Morozova *et al*., 2016a). Under acute ETOH, our model VTA circuit becomes more "synchronizable" and hence facilitates bursting. The mechanism of this boost in synchronization relies on a combination of several complementary effects: first, on the EtOH-mediated enhancement of AMPAR current that increases the probability to evoke spikes in response to the synchronous Glu pulses; second, on an increase in I_h, which renders the DA neurons intrinsically more sensitive to input synchrony (Morozova *et al*., 2016b); and third, on the possible ETOH-induced increase in GABAergic neurotransmission. The latter has a double effect in our model: the increased asynchronous inhibition outside the input bursts suppresses the tonic DA spikes, while the synchronized GABA input to the DA neuron during the input "bursts" promotes high frequency spikes in DA neurons.

In our model we focused on the input-induced synchronization of the VTA neurons. Further mechanisms of synchronization, such as gap junction coupling of DA neurons have been proposed (Grace and Bunney 1985). However, if gap junctions contribute strongly, they provide synchronization persisting at long intervals, especially with weak external inputs, which is not typically observed. At weaker gap junction connectivity, they play secondary role for synchronization and our results hold (see Supplementary materials). In addition to the gap junction coupling, another form of coupling between DA neurons may be through D2 dopamine autoreceptors that in turn modulate the GIRK-current in a dopamine-dependent manner (Ford et al. 2009). In order to verify how such coupling may affect our results, we simulated this effect by incorporating the D2-GIRK coupling to the DA neurons in our model (see Methods for model description). We observed that, as long as this coupling is not excessively strong, the qualitative DA dynamics we report above remain unchanged (see Fig. S1B).

We should be careful to point out that a distinction should be made between the reinforcing properties and the addictive properties of alcohol. While the former have indeed been related to the direct influence of alcohol on the mechanisms taking place in the VTA, the latter remains a challenge to understand from a neurobiological point of view and may not be directly related to the subjective hedonic impact of the drug. While classically mesolimbic dopamine signaling has been linked to the hedonic value (e.g. reward), recent works highlights its role in signaling motivational information and driving reinforcement-based learning. In this framework, ETOH-modulated DA signalling, specifically in the cortex, would result in pathological learning of the cortical representations of the motivational value for actions associated with obtaining ETOH and of the action-goal representation of the ETOH-linked environments and outcomes. Hence, ETOH-induced changes in the phasic DA output from the VTA may not be the direct cause of alcohol addiction, but a key component of the multi-faceted process of neuroadaptations and neuroplasticites that in the end produce the addicted behavior.

In conclusion, the circuit model here presented is able to reproduce the observed effect of EtOH on DA neuron activity and DA release. The model also makes testable predictions, specifically, the synchronization of DA neurons is proposed as the main mechanism for generation of transient peaks of DA concentration in NAc. Moreover, synchronization in cortical VTA afferents is proposed to be a fundamental ingredient for the increase in DA transients after EtOH injection. More generally, our model drives us to speculate that cortical activity states can determine potentially opposite effects of EtOH on DA response, varying from induced hyper-activation to a dose-dependent depression.

Aknowledgements

This work was supported by ANR grant "GABA" (BSG), by National Institute on Alcohol Abuse and Alcoholism (NIAAA) grant R01AA022821 (AK). BSG acknowledges support from the Russian Federal Program subsidy 5-100 to the NRU Higher School of Economics.

The authors declare no competing financial interests.

Author contributions

MD: performed research, drafted paper; EM: performed research; CL: designed research, drafted paper; AK: designed research, performed research, drafted paper; BSG: designed research, drafted paper.

Abberviations

VTA = Ventral Tegmental Area

pVTA = posterior Ventral Tegmental Area

PFC = Prefrontal Cortex

EtOH = Ethanol

Glu = Glutamatergic

DA = Dopamine

HCN = hyperpolarization-activated cyclic nucleotide–gated

GIRK = G protein-coupled inwardly-rectifying potassium channel

References

Allison, DW et al. (2006). Connexin-36 gap junctions mediate electrical coupling between ventral tegmental area GABA neurons. *Synapse*, *60*(1), 20-31.

Aryal, P., Dvir, H., Choe, S., & Slesinger, P.A. (2009) A discrete alcohol pocket involved in GIRK channel activation. *Nat. Neurosci*., 12, 988–995.

Baker SN, Spinks R, Jackson A, Lemon RN. (2001) Synchronization in monkey motor cortex during a precision grip task. I. Task-dependent modulation in single-unit synchrony. *Journal of Neurophysiology* 85(2):869-885.

Beier KT, Steinberg EE, DeLoach KE, Xie S, Miyamichi K, Schwarz L, Gao XJ, Kremer EJ, Malenka RC, Luo L (2015) Circuit Architecture of VTA Dopamine Neurons Revealed by Systematic Input-Output Mapping. *Cell.* 162(3):622-34

Blythe SN, Wokosin D, Atherton JF, Bevan MD. (2009) Cellular mechanisms underlying burst firing in substantia nigra dopamine neurons. *J Neurosci*. 29:15531–15541.

Blythe, Sarah N., Jeremy F. Atherton, and Mark D. Bevan. Synaptic activation of dendritic AMPA and NMDA receptors generates transient high-frequency firing in substantia nigra dopamine neurons in vitro. *Journal of neurophysiology* 97.4 (2007): 2837-2850.

Bourdy R, Barrot M. (2012) A new control center for dopaminergic systems: pulling the VTA by the tail. *Trends Neurosci*., 35, 681–690.

Brodie, M.S. & Appel, S.B. (1998) The effects of ethanol on dopaminergic neurons of the ventral tegmental area studied with intracellular recording in brain slices. *Alcohol. Clin. Exp. Res.*, 22, 236–244.

Buschman T J, et al. (2012) Synchronous oscillatory neural ensembles for rules in the prefrontal cortex. *Neuron* 76(4): 838-846.

Carr, D.B. & Sesack, S.R. (2000) Projections from the rat prefrontal cortex to the ventral tegmental area: target specificity in the synaptic associations with mesoaccumbens and mesocortical neurons. *J. Neurosci. Off. J. Soc. Neurosci.*, **20**, 3864–3873.

Carter, B.C., Giessel, A.J., Sabatini, B.L., & Bean, B.P. (2012) Transient sodium current at subthreshold voltages: activation by EPSP waveforms. *Neuron.*, 75, 1081–1093.

Chergui K, Charléty PJ, Akaoka H, Saunier CF, Brunet JL, Buda M, Svensson TH, Chouvet G (1993) Tonic activation of NMDA receptors causes spontaneous burst discharge of rat midbrain dopamine neurons in vivo. *Eur J Neurosci*. 5(2):137-44

Covey, D.P., Roitman, M.F., & Garris, P.A. (2014) Illicit dopamine transients: Reconciling actions of abused drugs. *Trends Neurosci.*, 37:200–210.

Deister, C.A., Teagarden, M.A., Wilson, C.J., & Paladini, C.A. (2009) An intrinsic neuronal oscillator underlies dopaminergic neuron bursting. *J. Neurosci.*, 29:15888–15897.

Ding Z-M, Engleman EA, Rodd ZA & McBride WJ, (2012) Ethanol increases glutamate neurotransmission in the posterior ventral tegmental area of female wistar rats. *Alcoholism: Clinical and Experimental Research* 36(4):633-40

Dehghani N. et al. (2016) Dynamic Balance of Excitation and Inhibition in Human and Monkey Neocortex. *Scientific reports* 6: 23176.

Dyr, W., et al., (1993) Effects of D1 and D2 dopamine receptor agents on ethanol consumption in the high-alcohol-drinking (HAD) line of rats. *Alcohol* 10(3):207-212

Durante, P., Cardenas, C.G., Whittaker, J.A., Kitai, S.T., & Scroggs, R.S. (2004) Low-threshold L-type calcium channels in rat dopamine neurons. *J Neurophysiol.*, 91, 1450–1454.

Eshel, N., Bukwich, M., Rao, V., Hemmelder, V., Tian, J., & Uchida, N. (2015) Arithmetic and local circuitry underlying dopamine prediction errors. *Nature*., **525**, 243–246.

Floresco SB, West AR, Ash B, Moore H, Grace AA. Afferent modulation of dopamine neuron firing differentially regulates tonic and phasic dopamine transmission. Nat Neurosci. 2003 Sep;6(9):968-73. PubMed PMID: 12897785.

Foddai M, Dosia G, Spiga S, Diana M. Acetaldehyde increases dopaminergic neuronal activity in the VTA. Neuropsychopharmacology. 2004 Mar; 29(3):530-6. PubMed PMID: 14973432.

Ford, Christopher P., Paul EM Phillips, and John T. Williams. "The time course of dopamine transmission in the ventral tegmental area." *Journal of Neuroscience* 29.42 (2009): 13344-13352.

Fonzi KM, Lefner MJ, Phillips PEM, Wanat MJ. (2017) Dopamine Encodes Retrospective Temporal Information in a Context-Independent Manner. Cell Rep. 20(8):1765-1774

Fujisawa S & Buzsáki G. (2011) A 4 Hz oscillation adaptively synchronizes prefrontal, VTA, and hippocampal activities. *Neuron* 72(1):153-165.

Galtieri DJ, Estep CM, Wokisin DL, Traynelis S, Surmier DJ (2017) Pedunculopontine glutamatergic neurons control spike patterning in substantia nigra dopaminergic neurons, eLife,

Gatto, G.J., McBride, W.J., Murphy, J.M., Lumeng, L., & Li, T.K. (1994) Ethanol self-infusion into the ventral tegmental area by alcohol-preferring rats. *Alcohol Fayettev. N.*, 11:557–564.

Gessa, Gian Luigi, et al. "Low doses of ethanol activate dopaminergic neurons in the ventral tegmental area." *Brain research* 348.1 (1985): 201-203.

Grace, A.A. & Bunney, B.S. (1984) The control of firing pattern in nigral dopamine neurons: burst firing. *J Neurosci*., 4, 2877–2890.

Grace, A. A., & Bunney, B. S. (1985). Dopamine. In *Neurotransmitter actions in the vertebrate nervous system* (pp. 285-319). Springer, Boston, MA.

Gonzales RA, Job MO, Doyon WM (2004) The role of mesolimbic dopamine in the development and maintenance of ethanol reinforcement.*Pharmacology & therapeutics* 103(2):121-146;

Joshua, M. et al. (2009). Synchronization of midbrain dopaminergic neurons is enhanced by rewarding events. *Neuron*, *62*(5): 695-704.

Ha, J. & Kuznetsov, A. (2013) Interaction of NMDA Receptor and Pacemaking Mechanisms in the Midbrain Dopaminergic Neuron. *PLoS ONE*., 8, 1–14.

Helton, T.D., Xu, W., & Lipscombe, D. (2005) Neuronal L-type calcium channels open quickly and are inhibited slowly. *J Neurosci*., 25, 10247–10251.

Hong, Simon, and Okihide Hikosaka. "Pedunculopontine tegmental nucleus neurons provide reward, sensorimotor, and alerting signals to midbrain dopamine neurons." *Neuroscience*282 (2014): 139-155

Keiflin, Ronald, and Patricia H. Janak. "Dopamine prediction errors in reward learning and addiction: from theory to neural circuitry." *Neuron* 88.2 (2015): 247-263

Kepler T., Marder E. Abbott, L. (1990) The effect of electrical coupling on the frequency of model neuronal oscillators. *Science* 248(4951): 83-85.

Kobayashi, T., Ikeda, K., Kojima, H., Niki, H., Yano, R., Yoshioka, T., & Kumanishi, T. (1999) Ethanol opens G-protein-activated inwardly rectifying K+ channels. *Nat. Neurosci*., 2, 1091–1097.

Kohler, M., Hirschberg, B., Bond, C.T., Kinzie, J.M., Marrion, N. V, Maylie, J., & Adelman, J.P. (1996) Small-conductance, calcium-activated potassium channels from mammalian brain. *Science*., 273, 1709–1714.

Lammel S et al. (2008) Unique properties of mesoprefrontal neurons within a dual mesocorticolimbic dopamine system. Neuron. 57(5): 760–773.

Lewohl, J.M., Wilson, W.R., Mayfield, R.D., Brozowski, S.J., Morrisett, R.A., & Harris, R.A. (1999) G-protein-coupled inwardly rectifying potassium channels are targets of alcohol action. *Nat. Neurosci*., 2, 1084–1090.

Li, Y.X., Bertram, R., & Rinzel, J. (1996) Modeling N-methyl-D-aspartate-induced bursting in dopamine neurons. *Neuroscience*., 71, 397–410.

Lin, John Y., et al. (2003) Dendritic projections and dye-coupling in dopaminergic neurons of the substantia nigra examined in horizontal brain slices from young rats. *Journal of neurophysiology* 90(4): 2531-2535.

Linsenbardt, D.N. & Lapish, C.C. (2015) Neural Firing in the Prefrontal Cortex During Alcohol Intake in Alcohol-Preferring "P" Versus Wistar Rats. *Alcohol. Clin. Exp. Res*., **39**, 1642–1653.

Lobb, C.J., Wilson, C.J., & Paladini, C.A. (2010) A Dynamic Role for GABA Receptors on the Firing Pattern of Midbrain Dopaminergic Neurons. *J. Neurophysiol*., **104**, 403–413.

McDaid, J., McElvain, M.A., & Brodie, M.S. (2008) Ethanol Effects on Dopaminergic Ventral Tegmental Area Neurons During Block of I_h: Involvement of Barium-Sensitive Potassium Currents. *J. Neurophysiol*., 100, 1202–1210.

Mereu, G., Fadda, F., & Gian Luigi Gessa (1984) Ethanol stimulates the firing rate of nigral dopaminergic neurons in unanesthetized rats. *Brain Res*., 292, 63–69.

Margolis E. B., et al. (2012) Identification of rat ventral tegmental area GABAergic neurons. *PloS one* 7(7): e42365

Mokdad, Ali H., et al. (2004) Actual causes of death in the United States, 2000.*Jama*291(10): 1238-1245.

Morikawa, H. & Morrisett, R.A. (2010) Ethanol action on dopaminergic neurons in the ventral

tegmental area: interaction with intrinsic ion channels and neurotransmitter inputs. *Int. Rev. Neurobiol.*, 91, 235–288.

Morozova, E.O. et al. (2016a) Contribution of synchronized GABAergic neurons to dopaminergic neuron firing and bursting. *J. Neurophysiol.*, 116, 1900–1923.

Morozova, E.O., Zakharov, D., Gutkin, B.S., Lapish, C.C., & Kuznetsov, A. (2016b) Dopamine Neurons Change the Type of Excitability in Response to Stimuli Blackwell, K.T., (ed). *PLOS Comput. Biol.*, 12, e1005233.

Okada, K.-i., Toyama, K., Inoue, Y., Isa, T., and Kobayashi, Y. (2009). Different Pedunculopontine Tegmental Neurons Signal Predicted and Actual Task Rewards. *Journal of Neuroscience*, 29(15):4858–4870.

Okamoto, T., Harnett, M.T., & Morikawa, H. (2006) Hyperpolarization-activated cation current (Ih) is an ethanol target in midbrain dopamine neurons of mice. *J. Neurophysiol.*, 95, 619–626.

Okun M., Naim A. & Lampl I. (2010) The subthreshold relation between cortical local field potential and neuronal firing unveiled by intracellular recordings in awake rats. *Journal of neuroscience* 30(12): 4440-4448.

Oster A. M., & Gutkin, B. S. (2011). A reduced model of DA neuronal dynamics that displays quiescence, tonic firing and bursting. *Journal of Physiology-Paris*, *105*(1):53-58.

Overton P, Clark D (1992) Iontophoretically administered drugs acting at the N-methyl- D-aspartate receptor modulate burst firing in A9 dopamine neurons in the rat. *Synapse.* 10(2):131-40

Paladini, C. A., & Roeper, J. (2014). Generating bursts (and pauses) in the dopamine midbrain neurons. *Neuroscience*, *282*, 109-121

Pan, Wei-Xing, and Brian I. Hyland. "Pedunculopontine tegmental nucleus controls conditioned responses of midbrain dopamine neurons in behaving rats." *Journal of Neuroscience*25.19 (2005)

Pierce, C. R., & Kumaresan V, (2006) The mesolimbic dopamine system: the final common pathway for the reinforcing effect of drugs of abuse? *Neuroscience & biobehavioral reviews* 30(2):215-238.

Ping, H.X. & Shepard, P.D. (1996) Apamin-sensitive Ca2+-activated K+ channels regulate pacemaker activity in nigral dopamine neurons: *NeuroReport*., **7**, 809–814.

Plassmann, Hilke, John P. O'Doherty, and Antonio Rangel. "Appetitive and aversive goal values are encoded in the medial orbitofrontal cortex at the time of decision making." *Journal of neuroscience* 30.32 (2010): 10799-10808.

Reyes, A.(2001) Influence of dendritic conductances on the input-output properties of neurons. *Annual review of neuroscience*, *24*(1):653-675.

Richards, C.D., Shiroyama, T., & Kitai, S.T. (1997) Electrophysiological and immunocytochemical characterization of GABA and dopamine neurons in the substantia nigra of the rat. *Neuroscience*., **80**, 545–557.

Rodd, Z.A., Bell, R.L., Melendez, R.I., Kuc, K.A., Lumeng, L., Li, T.-K., Murphy, J.M., & McBride, W.J. (2004) Comparison of intracranial self-administration of ethanol within the posterior ventral tegmental area between alcohol-preferring and Wistar rats. *Alcohol. Clin. Exp. Res*., 28, 1212–1219

Roeper J. (2013) Dissecting the diversity of midbrain dopamine neurons. *Trends in neurosciences* 36(6):336-342.

Saal, D., Dong, Y., Bonci, A., & Malenka, R.C. (2003) Drugs of abuse and stress trigger a common synaptic adaptation in dopamine neurons. *Neuron*., 37, 577–582.

Schacht, Joseph P., Raymond F. Anton, and Hugh Myrick. "Functional neuroimaging studies of alcohol cue reactivity: a quantitative meta-analysis and systematic review." *Addiction biology* 18.1 (2013): 121-133.

Samson H. H., et al. , (1993) Effect of dopamine agonists and antagonists on ethanol-reinforced behavior: the involvement of the nucleus accumbens. *Brain research bulletin* 30(1-2): 133-143

Seamans, Jeremy K., and Charles R. Yang. "The principal features and mechanisms of dopamine modulation in the prefrontal cortex." *Progress in neurobiology* 74.1 (2004): 1-58.

Steffensen, Scott C., et al. (1998) Electrophysiological characterization of GABAergic neurons in the ventral tegmental area. *Journal of neuroscience* 18(): 8003-8015

Stobbs, S.H., et al. (2004) Ethanol suppression of ventral tegmental area GABA neuron electrical transmission involves N-methyl-D-aspartate receptors. *Journal of Pharmacology and Experimental Therapeutics* 311(1): 282-289.

Tateno, T., & Robinson, H. P. (2011). The mechanism of ethanol action on midbrain dopaminergic neuron firing: a dynamic-clamp study of the role of I(h) and GABAergic synaptic integration. *Journal of neurophysiology*, *106*(4), 1901-1922.

Theile JW, Morikawa H, Gonzales RA, Morrisett RA, (2008) Ethanol enhances GABAergic transmission onto dopamine neurons in the ventral tegmental area of the rat. *Alcohol Clin Exp Res* 32(6):1040–1048

Tu Y et al. (2007) Ethanol inhibits persistent activity in prefrontal cortical neurons. *Journal of Neuroscience* 27(17): 4765-4775.

van Zessen R, Phillips JL, Budygin EA, Stuber GD. (2012) Activation of VTA GABA neurons disrupts reward consumption. *Neuron* 73, 1184–1194.

Wang X.J. and Buzsáki G. Gamma oscillation by synaptic inhibition in a hippocampal interneuronal network model. *The journal of Neuroscience* 16.20 (1996): 6402-6413

Weiner J. L., & Valenzuela C. F. (2006). Ethanol modulation of GABAergic transmission: the view from the slice. *Pharmacology & therapeutics*, *111*(3):533-554.

Wightman, R. M., and Zimmerman J.B. Control of dopamine extracellular concentration in rat striatum by impulse flow and uptake. *Brain research reviews* 15.2 (1990): 135-144.

Wilson, C. J., & Callaway, J. C. (2000) Coupled oscillator model of the dopaminergic neuron of the substantia nigra. *Journal of neurophysiology*, *83*(5):3084-3100.

Xiao, C., Shao, X.M., Olive, M.F., Griffin, W.C., Li, K.-Y., Krnjevi, K., Zhou, C., & Ye, J.-H. (2009) Ethanol Facilitates Glutamatergic Transmission to Dopamine Neurons in the Ventral Tegmental Area. *Neuropsychopharmacology*., **34**, 307–318.

Yim, H. J., & Gonzales, R. A. (2000). Ethanol-induced increases in dopamine extracellular concentration in rat nucleus accumbens are accounted for by increased release and not uptake inhibition. *Alcohol*, *22*(2):107-115.

Table 1: Model parameters

PARAMETER	DESCRIPTION	VALUE
c_m	Membrane capacitance of DA and GABA neurons	$1\mu F/cm^2$
$\bar{g}_K$	Maximal potassium conductance on DA neuron	$1mS/cm^2$
$\bar{g}_{Ca}$	Maximal calcium conductance on DA neuron	$2.5mS/cm^2$
$\bar{g}_{KCa}$	Maximal calcium-dependent potassium conductance on DA neuron	$7.8mS/cm^2$
$\bar{g}_{sNa}$	Maximal subthreshold sodium conductance on DA neuron	$0.13mS/cm^2$
g_l	Leak conductance on DA neuron	$0.18mS/cm^2$
$\bar{g}_{Na}$	Maximal sodium conductance on DA neuron	$50mS/cm^2$

$\bar{g}_{Nag}$	Maximal sodium conductance on GABA neuron	22mS/cm^2
$\bar{g}_{Kg}$	Maximal potassium conductance on GABA neuron	7mS/cm^2
$\bar{g}_{AMPA,GABA}$	AMPA conductance on GABA neurons	0.8mS/cm^2
$\bar{g}_{NMDA,GABA}$	NMDA conductance on GABA neurons	0.5mS/cm^2
g_{el}	Gap junction coupling between GABA neurons	0.02mS/cm^2
$\bar{g}_{NMDA,DA}$	Maximal NMDA conductance on DA neuron	18mS/cm^2
E_h	HCN reversal potential on DA neuron	-20 mV
E_K	Potassium reversal potential on DA and GABA neurons	-90 mV
E_{Ca}	Calcium reversal potential on DA neuron	50 mV
E_{Na}	Sodium reversal potential on DA and GABA neurons	55 mV
E_l	Leak reversal potential on DA neuron	-35 mV
E_{lg}	Leak reversal potential on GABA neuron	-51 mV
E_{NMDA}	NMDA reversal potential on DA and GABA neurons	0 mV
E_{AMPA}	AMPA reversal potential on DA and GABA neurons	0 mV
E_{GABA}	GABA reversal potential on DA neuron	-90 mV
τ_{act}	AMPA receptor activation time on DA and GABA neurons	1 ms
τ_{deact}	AMPA receptor deactivation time on DA and GABA neurons	1.6 ms

τ_{des}	AMPA receptor desensitization time	6.1 *ms*
τ_{desrel}	AMPA receptor release from desensitization time	40 *ms*
τ_{nact}	NMDA receptor activation time on DA and GABA neurons	7 *ms*
τ_{ndeact}	NMDA receptor deactivation time on DA and GABA neurons	170 *ms*
τ_{gact}	GABA receptor activation time on DA and GABA neurons	0.08 *ms*
τ_{gdeact}	GABA receptor deactivation time on DA and GABA neurons	10 *ms*
$P_0(g_h)$	HCN maximal conductance at zero EtOH concentration	0.2 mS/cm^2
$P_M(g_h)$	HCN maximal conductance at 3g/Kg EtOH concentration	0.8 mS/cm^2
$P_0(g_{GIRK})$	GIRK maximal conductance at zero EtOH concentration	0.08 mS/cm^2
$P_M(g_{GIRK})$	GIRK maximal conductance at 3g/Kg EtOH concentration	0.1 mS/cm^2
$P_0(g_{AMPA,DA})$	AMPA maximal conductance at zero EtOH concentration	3 mS/cm^2
$P_M(g_{AMPA,DA})$	AMPA maximal conductance at 3g/Kg EtOH concentration	12 mS/cm^2
$P_0(g_{GABA})$	GABA maximal conductance at zero EtOH concentration	1.2 mS/cm^2
$P_M(g_{GABA})$	GABA maximal conductance at 3g/Kg EtOH concentration	4.8 mS/cm^2

Supplementary material

S1. Effect of DA coupling and NMDA block

We report the effects of NMDA blockade (Fig. S1 A1-A2), D2 receptor (Fig. S1 B1-B2) and electrical coupling between DA neurons (Fig. S1 C1-C2) on the EtOH dependent DA neurons activity. As discussed in the main text these results show that DA bursting is sustained by NMDA and that the results are not qualitatively affected by electrical or D2 coupling as long as these currents are not too strong.

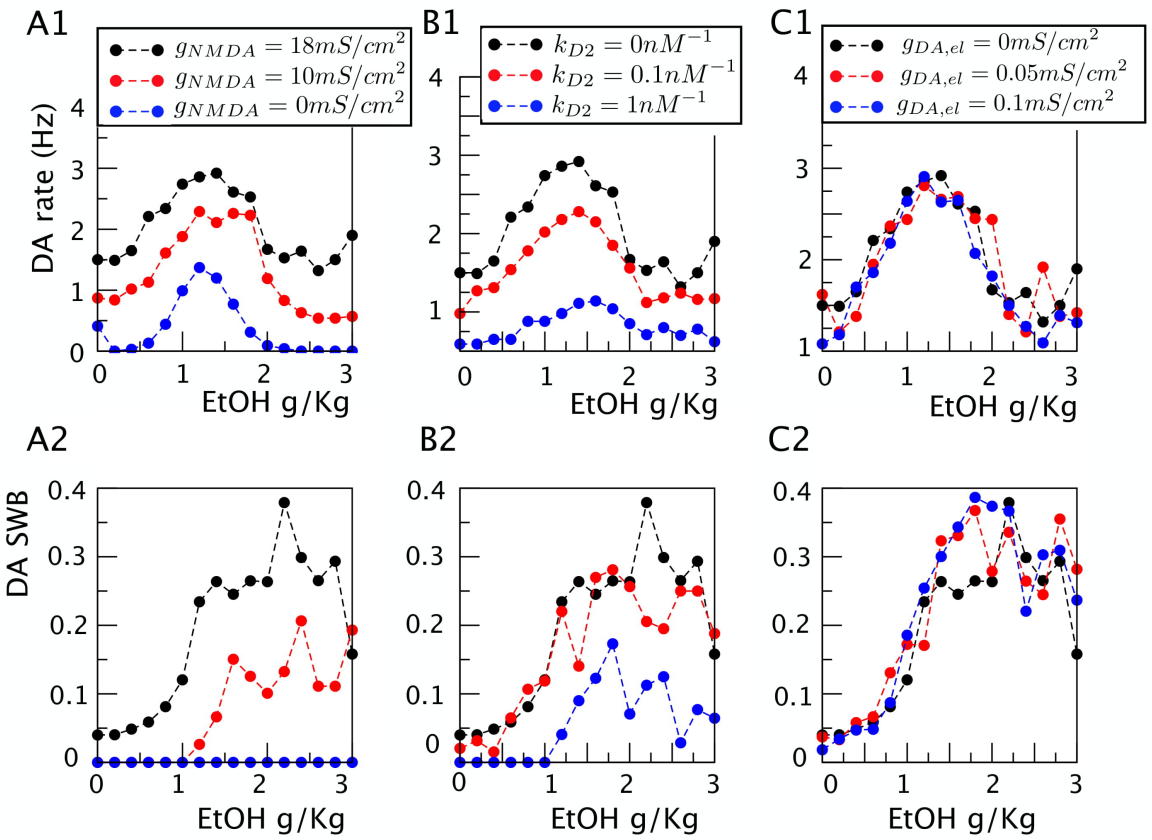

Figure S1: **Bursting is NMDA-mediated and DA neurons coupling (D2 receptors gap-junction) do not affect qualitatively EtOH effects**

(A) DA firing rate (A1) and SWB (A2) as a function of EtOH concentration for different values of NMDA conductance on DA neurons (black control 18mS/cm^2, red 9mS/cm^2, blue zero). (B) DA firing rate (B1) and SWB (B2) as a function of EtOH concentration for different D2 receptor modulation by DA k_{D2} (black control 0nM^{-1}, red 0.1nM^{-1}, blue 1nM^{-1}). (C) DA firing rate (C1) and SWB (C2) as a function of EtOH concentration for different electrical coupling strength between DA neurons $g_{DA,el}$ (black control 0mS/cm^2, red 0.05mS/cm^2, blue 0.1mS/cm^2). Please note that all other model parameters are the same as in Fig3C-D of the main text.

S2. DA neuron model details

Two currents comprise the intrinsic pacemaking mechanism in DA neuron model: an L-type voltage-dependent calcium current $I_{Ca} = g_{Ca}(E_{Ca}\text{-}v)$ and an SK-type calcium-dependent potassium current $I_{K,Ca} = g_{K,Ca}(E_{K,Ca}\text{-}v)$. Gating of the calcium current is instantaneous (Wilson & Callaway, 2000; Helton *et al*., 2005) and described by the function

$$g_{Ca} = \overline{g_{Ca}} \frac{\alpha_c^4(v)}{\alpha_c^4(v) + \beta_c^4(v)}$$

Calibration of the calcium gating function reflects an activation threshold of an L-type current around -50mV, which is significantly lower in DA neurons than in other neurons (Wilson & Callaway, 2000; Durante *et al*., 2004). A large influx of Ca^{2+} leads to activation of the SK current, which contributes to repolarization of the DA neuron. Dependence of the SK conductance on calcium concentration is modeled as follows (Kohler *et al*., 1996)

$$g_{K,Ca} = \overline{g_{K,Ca}} \frac{[Ca^{2+}]^4}{[Ca^{2+}]^4 + [K^+]^4}$$

Calcium concentration varies according to the following equation:

$$\frac{d[Ca^{2+}]}{dt} = \frac{2\beta}{r}\left(\frac{g_{Ca}(v) + 0.1g_l}{zF}(E_{Ca}\text{-}v)\text{-}P_{Ca}u\right)$$

This equation represents balance between Ca^{2+} entry via the L channel and the leak current, and Ca^{2+} removal via a pump. In the calcium equation, β is the calcium buffering coefficient (β=0.00023), i.e. the ratio of free to total calcium, r is the radius of the compartment (r=0.2μm), z is the valence of calcium, and F is Faraday's constant. P_{Ca} represents the maximum rate of calcium removal through the pump (P_{Ca}=1923μm/s). The model is calibrated according to our previous paper (Morozova *et al*., 2016a).

The neuron is repolarized by the activation of a large family of voltage-gated potassium channels. The model contains voltage-dependent K^+ current $I_K = g_K(E_K\text{-}v)$. Conductance of this current is given by a Boltzmann function:

$$g_K = \overline{g_K} \frac{1}{1 + \exp\left(-\frac{v+10}{7}\right)}$$

The DA neuron expresses voltage gated sodium channels that carry a large transient current during action potentials (the spike-producing sodium current and a non-inactivating current present at subthreshold voltages (a subthreshold sodium current $I_{sNa} = g_{sNa}(E_{sNa}\text{-}v)$. Even though the persistent subthreshold sodium current is much smaller than the transient spike-producing current, it influences the firing pattern and the frequency of the DA neuron by contributing to depolarization below the spike threshold. We modeled the voltage dependence of the subthreshold sodium current as follows

$$g_{sNa} = \overline{g_{sNa}} \frac{1}{1 + \exp\left(-\frac{v+50}{5}\right)}$$

The kinetics and the voltage dependence of the subthreshold sodium current were taken from (Carter *et al*., 2012). The spike-producing sodium current has the form of Hodgkin-Huxley model $I_{Na} = g_{Na} m^3 h(E_{Na}\text{-}v)$, where sodium activation and inactivation channels obey the following differential equations:

$$\frac{dm}{dt} = \alpha_m(v)(1\text{-}m)\text{-}\beta_m(v)m$$

$$\frac{dh}{dt} = \alpha_h(v)(1\text{-}h)\text{-}\beta_h(v)h$$

where the rate constants α_x and β_x have the following form:

$$\alpha_m = \frac{0.1(v+25)}{\exp\left(\frac{v+25}{10}\right)\text{-}1}; \beta_m = 4\exp\left(v/18\right)$$

$$\alpha_h = 0.07\exp(v/20);\ \beta_h = \frac{1}{\exp\left(\frac{v+30}{10}\right)+1}$$

The leak current $I_l = g_l(E_l\text{-}v)$ in the model has the reversal potential of -35 mV, which is higher than in the majority of neuron types. In DA neurons, several types of depolarizing, nonselective cation currents are expressed, which likely contribute to depolarization during interspike intervals.

The GIRK current is modeled as a potassium current and is described in Methods section. The HCN channel $I_h = g_h q(E_h\text{-}v)$ depends on the activation variable q that obeys the following differential equation (Tateno et al. 2011):

$$\frac{dq}{dt} = \frac{q\text{-}Q(v)}{\tau_q(v)}$$

$$Q(v) = \frac{1}{1 + \exp\left(\frac{v+70}{10}\right)}$$

$$\tau_q(v) = 320 + 1850exp(-\frac{v+80}{18})$$

where, in the last equation, constants are measured in ms.

S3. GABA neuron model

GABA neuron dynamics obeys the following differential equations:

$$c_m \frac{dv}{dt} = g_{Na}m^3h(E_{Na}\text{-}v) + g_K n^4(E_K\text{-}v) + g_{lg}\left(E_{lg}\text{-}v\right) + I_{el} + I_{syn}$$

$$\frac{dn}{dt} = \alpha_n(v)(1\text{-}n)\text{-}\beta_n(v)n$$

$$\frac{dh}{dt} = \alpha_h(v)(1\text{-}h)\text{-}\beta_h(v)h$$

where v is the voltage of cell, I_{el} is the electrical coupling with the other neurons and I_{syn} is the synaptic coupling with external Glutamatergic inputs (see A1.1). The activation variable equations are completed by the following relations:

$$m = \frac{\alpha_m}{\alpha_m + \beta_m}$$

$$\alpha_m = \frac{0.1(v+30)}{1\text{-}\exp\left(-\frac{v+30}{10}\right)};\ \beta_m = 4\exp\left(-\frac{v+55}{18}\right)$$

$$\alpha_h = 0.01\exp\left(-\frac{v+47}{18}\right);\ \beta_h = \frac{1}{1 + \exp\left(-\frac{v+23}{10}\right)}$$

$$\alpha_n = \frac{0.01(v+29)}{1\text{-}\exp\left(-\frac{v+29}{10}\right)};\ \beta_n = 0.0875\exp\left(-\frac{v+39}{80}\right)$$